Chapter 6

Rheological Properties of Carbon Nanofiber-Filled Polyamide Composites and Blend of these Composites and TPE

Yosuke Nishitani and Takeshi Kitano

Additional information is available at the end of the chapter

http://dx.doi.org/10.5772/64531

Abstract

For the purpose of developing new engineering materials with sufficient balance among mechanical, electrical, processability, triboloical properties, etc., in this study, we investigated the dynamic viscoelastic properties of carbon nanofiber (CNF) filled polyamide (PA) composites and the blend of these composites and thermoplastic elastomer (TPE) in the molten state, which were mainly obtained in our previous studies. It was found that vapor grown carbon fiber (vapor grown carbon fiber) has a stronger influence on the dynamic viscoelastic properties of the composites in the molten state. Rheological percolation thresholds seem to exist between 1vol.% and 5vol. % of VGCF contents. On the other hand, the effect of the addition of TPE (styrene-ethylene/butylene-styrene copolymer (SEBS) and maleic anhydride grafted SEBS (SEBS-g-MA)) on the dynamic viscoelastic properties of VGCF/PA6 composites in the molten state differed at each viscoelastic value. It was clarified that the dynamic viscoelastic properties of VGCF/PA6/SEBS-g-MA ternary composites are higher than those of VGCF/PA6/SEBS ones. Furthermore, the influence of processing sequences on the dynamic viscoelastic properties of VGCF/PA6/SEBS-g-MA composites in the molten state differed according to the mixing steps of materials. These may be attributed to the change in the internal structure caused by addition of TPE, type of SEBS and processing sequences.

Keywords: dynamic viscoelastic properties in molten state, carbon nanofiber, polyamide, composites, polymer blends

1. Introduction

Recently, nanofiller-filled thermoplastic composites are attracting considerable interest [1–5]. One of the advantages of these nanocomposites is that the volume ratio of the fillers in the systems is much lower than that of conventional thermoplastic composites, offering a distinct advantage in that less energy is required when these nanocomposites are processed for industrial applications. Graphitic carbon nanofilaments such as single-wall carbon nanotube (SWCNT) and carbon nanofiber (CNF) have been of great research interest [6, 7]. Especially, CNF-filled thermoplastic composites have been proven to be very beneficial in terms of the improved mechanical, thermal, and electrical properties [8–14]. CNF disperses well in the polymer matrix and has a diameter of about 100–150 nm, which is relatively larger than other nanofilaments. It can therefore serve as a low-cost alternative to SWCNT. In our previous works, we investigated the rheological, mechanical, and tribological properties of various carbon fibers (CFs) such as polyacrylonitrile-based carbon fiber (PAN-CF) and pitch-based carbon fiber (Pitch-CF) and two kinds of vapor grown carbon fiber (VGCF and VGCF-S) and filled thermoplastic (polyamide (PA), polybutylene terephthalate (PBT), etc.) [15–22] composites in order to obtain new polymer nanocomposite-based engineering materials for use as the structural materials and tribomaterials of mechanical sliding parts such as gears, bearings, cams, seals, etc. The mechanical and tribological properties improved when filled with various CFs. Fiber properties such as aspect ratio (length/diameter) and fiber diameter have a stronger influence on the viscoelastic properties than fiber content. We also demonstrated the optimum mechanical and tribological properties of various CF-filled polymer composites. However, to further enhance the mechanical, electrical, processability, tribological properties, etc. in these CNF-filled thermoplastic composites, it is very critical to understand the rheological behavior of these thermoplastic composites in the molten state such as processability, internal microstructure, changes, and structure-property relationships [23–25].

Moreover, to date, little interest has been paid to multicomponent polymer composites such as polymer blends based on CNF-filled thermoplastic composites for engineering materials [18, 22, 26, 27]. To develop new engineering materials with sufficient balance among mechanical, electrical, processability, tribological properties, etc., various properties need to be well balanced. Several investigations have proved that multicomponent polymer composites, which are ternary blends based on nanofiller-filled composites such as nanofiller/polymer/polymer or nanofiller/polymer/rubber, etc., are effective for realizing good balances among various properties [18, 22, 26–32]. Above all, their remarkable performance stems from their morphologies in immiscible blends. It is well known that the morphologies of immiscible polymer blends are controlled by the chemical reaction between components during melt blending [32]. In addition, the morphologies of multicomponent polymer composites such as phase structure, fiber dispersion, fiber localization, etc. are strongly influenced by the design of material composition and by the processing sequence of melt mixing using a twin extruder. The former is the material design of multicomponent materials: specifically, the type of materials, composition ratio, whether compatibilizer is used or not, functional groups, surface treatment of filler, etc. [32, 33]. On the other hand, the latter is the mixing technique of multicomponent composites [22, 34, 35]. The processing sequences during melt mixing using

http://dx.doi.org/10.5772/64531

a twin screw extruder affect the morphologies of multicomponent composites. As a result, the physical properties are also strongly influenced by the processing sequence. However, there are only a few published studies on the effects of the addition of thermoplastic elastomer (TPE) and the processing sequence on dynamic viscoelastic properties of these CNF-filled multicomponent composites [18]. For the purpose of developing new engineering materials with sufficient balance among mechanical, electrical, processability, tribological properties, etc., we investigated the dynamic viscoelastic properties of CNF-filled polyamide composites and the blend of these composites and TPE in the molten state, which were obtained mainly in our previous studies. In particular, this study discusses the effects of the filling of CNF, addition of TPE, and processing sequence on dynamic viscoelastic properties in the molten state.

2. Dynamic viscoelastic properties of carbon nanofiber-filled polyamide 66 composites in the molten state

2.1. Introduction

CNF is nanosized diameter CF and is used as fillers for polymer composites. One of the advantages of CNF-filled composites is that the volume ratio of fillers in the systems is much lower than that of conventional polymer composites. These CNF-filled polymer composites have been proven to be very beneficial in terms of improved mechanical, electrical, tribological properties, etc. [5, 8–14]. In our previous studies, we investigated the mechanical and tribological properties of various vapor grown carbon fibers (VGCF), which are a type of CNF-filled polymer composites: polyamide (PA) [20–22], polybutylene terephthalate (PBT) [15, 17–19], polyimide (PI) [16], etc. were used as matrix polymer. We found that the mechanical and tribological properties improved when filled with VGCF, and demonstrated the optimum mechanical and tribological properties for various VGCF-filled polymer composites. However, to further enhance the mechanical, electrical, processability, tribological properties, etc. in these CNF-filled thermoplastic composites, it is critical to understand the rheological behavior of these composites in the molten state such as processability, internal microstructure, changes, and structure-property relationships [23–25]. Several studies have proven that VGCF-filled polymer composites such as VGCF/polycarbonate (PC) [8, 10], VGCF/polypropylene (PP) [10, 11, 36], VGCF/polystyrene (PS) [37], VGCF/PBT [15, 19], etc. demonstrate distinctive rheological behaviors. However, there is still a lack of comprehensive understanding of the rheological properties of these VGCF-filled composites, in particular, when VGCF content is low. The purpose of this study is to experimentally investigate the rheological properties, which is the dynamic viscoelastic properties in the molten state, of VGCF/PA66 composites. Particularly, this study discusses the effect of the filling of VGCF, volume fraction, strain, angular frequency, and temperature on the dynamic viscoelastic properties in the molten state.

2.2. Materials and methods

The materials used in this study were carbon nanofiber (CNF)-filled polyamide 66 (PA66) composites in the molten state, which are used in the first step of the fabrication of these

composites. PA66 (UBE Nylon 2020P, Ube Industries, Ltd., Japan) was used as the matrix polymer. Vapor grown carbon fiber (Showa Denko K. K., Japan) which is a type of CNF was used as the filler. Its fiber diameter and initial length are 150 nm and 10 μm, respectively. VGCF-filled PA66 composites (VGCF/PA66) with the VGCF content of 1, 5, and 10 vol% were prepared in this study. All the components were dried for 5 h at 100°C in a vacuum oven beforehand until the moisture level was 0.2%, then dry blended in a small bottle, and subsequently the melt was mixed at 110 rpm and 295°C in a twin screw extruder (TEX-30, Japan Steel Works, Ltd., Japan). After mixing, the extruded strands of VGCF/PA66 composites were cut into 5 mm long pieces by the pelletizer, and dried again for 5 h at 100°C in a vacuum oven. In addition, 1 mm thick sheets were compression molded at the conditions of 270°C, 5 MPa, and 3 min, and cut into ϕ25 mm disk shapes for measuring the rheological properties. The rheological properties in the molten state were evaluated by oscillatory flow testing using a parallel plate-type rotational rheometer (ARES, Rheometric Scientific Co., USA and ARES-G2, TA Instruments Japan Inc., Japan). The diameter of the parallel plate was ϕ25 mm, and the gap between the two plates was fixed at 1 mm. Under such gap conditions, the test specimens were slightly compressed in the molten state. First, the strain sweep test was performed from initial strain value 10^{-1} to a final strain value of 10^{2} in percent at the angular frequency of 3.5 rad/s. Second, in frequency sweep testing, a small strain amplitude oscillatory shear was applied to the sample. The angular frequency was varied from 10^{-1} to 10^{2} rad/s, and the strain amplitude was set as 1%. These measurements were carried out for all samples at 270, 280, and 290°C. The dynamic viscoelastic properties in the molten state were evaluated by storage modulus G', loss modulus G'', loss tangent tan δ, phase angle δ (= arctan G''/G'), complex modulus $|G^*|$, and complex viscosity $|\eta^*|$.

2.3. Strain dependences

Viscoelastic properties of VGCF/PA66 composites are discussed in this section. First, strain sweep testing was carried out to characterize the strain dependence of viscoelastic properties and also transition from linear to nonlinear viscoelastic ones of VGCF/PA66 composites and then to estimate the change in the internal microstructure of these composites. Since the storage modulus G' is a more sensitive rheological function to the structural changes of the nanocomposites than the loss modulus G'', only the storage modulus curves are presented in this study [38]. The strain dependence of the storage modulus G' of VGCF/PA66 composites is shown in **Figure 1**. This measurement was carried out for all samples at 280°C and the angular frequency of ω at 3.5 rad/s. The strain dependences of G' show remarkably different behavior according to the volume fraction of VGCF V_f. The G' of neat PA66 (100%) and VGCF/PA66 with V_f= 1 vol % (VGCF1) exhibits a linear behavior, in which the modulus is a constant over a wide range of strain amplitude. On the other hand, the G' of VGCF/PA66 with V_f = 5 vol% (VGCF5) and V_f = 10 vol% (VGCF10) show linear plateau only in low strain regions and rapidly decrease with increasing strain, which is an independent transition from linear to nonlinear behavior. It was observed that the value of the plateau modulus G'_p changes with increasing V_f. These results may be due to the increase in the fiber-matrix interactions, and to the increase in the surface area of fiber with increasing V_f.

http://dx.doi.org/10.5772/64531

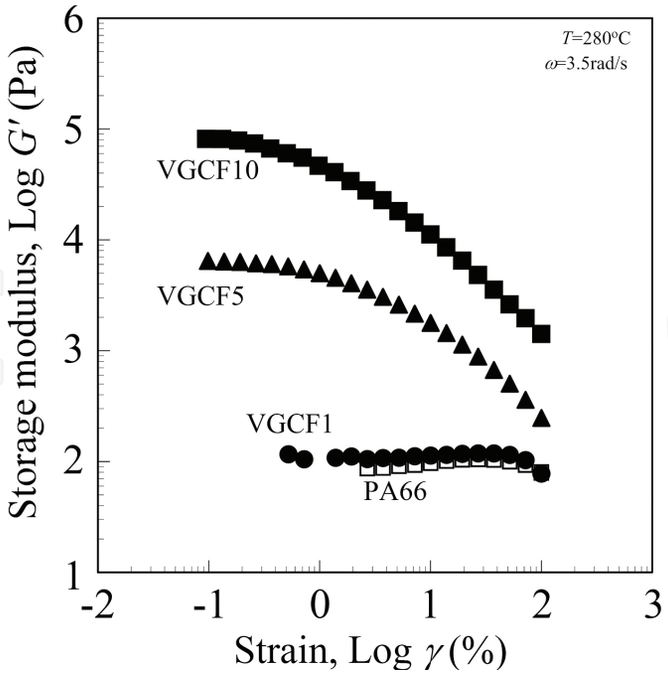

Figure 1. Storage modulus as function of strain for VGCF/PA66 composites at 3.5 rad/s and 280°C.

To clarify the transition point from linear to nonlinear behavior, the strain dependences of relative storage modulus G'_r (= G'/G'_p) of VGCF/PA66 composites are shown in **Figure 2**. Here, the relative storage modulus G'_r is given by the values of VGCF/PA66 composites divided by that of the G'_p of VGCF/PA66 composites. The regions of linear viscoelastic behavior for neat PA66 and VGCF1 are clearly observed over a whole range of strain. However, those of VGCF5 and VGCF10 decrease abruptly in the G'_r, which shows nonlinear behavior. The transition point which appeared in the deviation region from linear to nonlinear viscoelastic behavior is defined as critical strain γ_c. γ_c was generally taken as the strain value at the G' equal to 90% of the plateau modulus (0.9 G'_p) [19, 38], which is shown in the broken line in **Figure 2**. The relationship between critical strain value γ_c and volume fraction of fiber V_f of VGCF/PA66 composites at 3.5 rad/s and 280°C is shown in **Figure 3**. γ_c of VGCF/PA66 composites varies sharply from V_f, and exhibits a straight relation between γ_c and V_f on this log-log plot. That is power law of γ_c and V_f ($\gamma_c \propto V_f^{\,n}$). Here, n is the slope of power law and is found to be –2.55 from the relation in **Figure 3**. This may be attributed to the change in the internal structure of the composites such as fiber dispersion, fiber-matrix, and fiber-fiber interactions caused by increasing V_f [19, 39]. In general, it is well known that the dependence of critical strain value on the volume fraction of fiber of polymer composites and nanocomposites can be explained in terms of the change of internal microstructure formation, the alignment of the anisotropic nanofiller to the strain direction, and the breakdown of fiber-fiber interaction of the physical networks [19, 32, 38]. These behaviors have been reported for other nanofillers such as clay, silica, etc. filled polymer nanocomposites [39, 40]. In this study, it was found that the volume fraction of fiber has a strong influence on the strain dependence of viscoelastic properties.

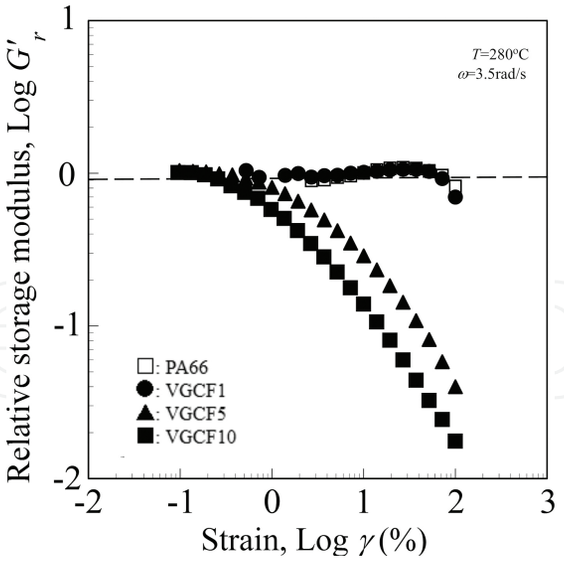

Figure 2. Relative storage modulus as function of strain for VGCF/PA66 composites at 3.5 rad/s and 280°C.

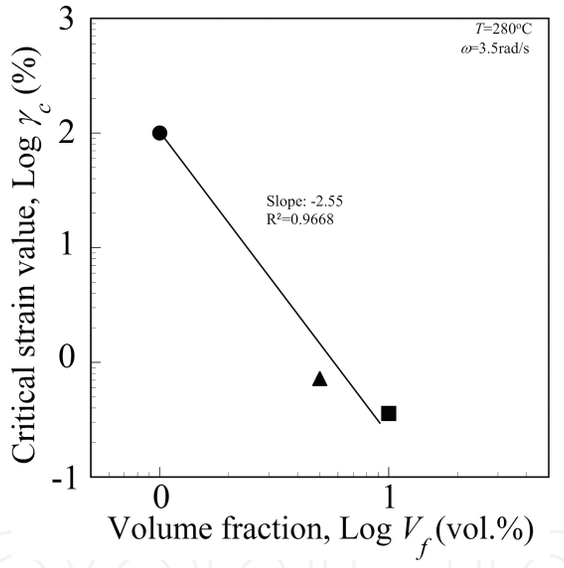

Figure 3. Dependence of critical strain on volume fraction of VGCF for VGCF/PA66 composites at 3.5 rad/s and 280°C.

2.4. Angular frequency dependences

The rheological properties of VGCF/PA66 composites were evaluated by oscillatory flow behavior, which are considered to be strongly dependent on the internal microstructure of these composites. The dynamic viscoelastic properties of these composites are plotted as a function of angular frequency ω at 280°C and strain of 1% in **Figure 4(a)** (storage modulus G'), **Figure 4(b)** (loss modulus G''), **Figure 4(c)** (loss tangent tan δ), and **Figure 4(d)** (complex viscosity $|\eta^*|$), respectively. The slope of G' and G'' against ω in low and high ω regions are listed in **Table 1**. The G' of neat PA66 increases with increasing ω; however, the slope of G'- ω

http://dx.doi.org/10.5772/64531

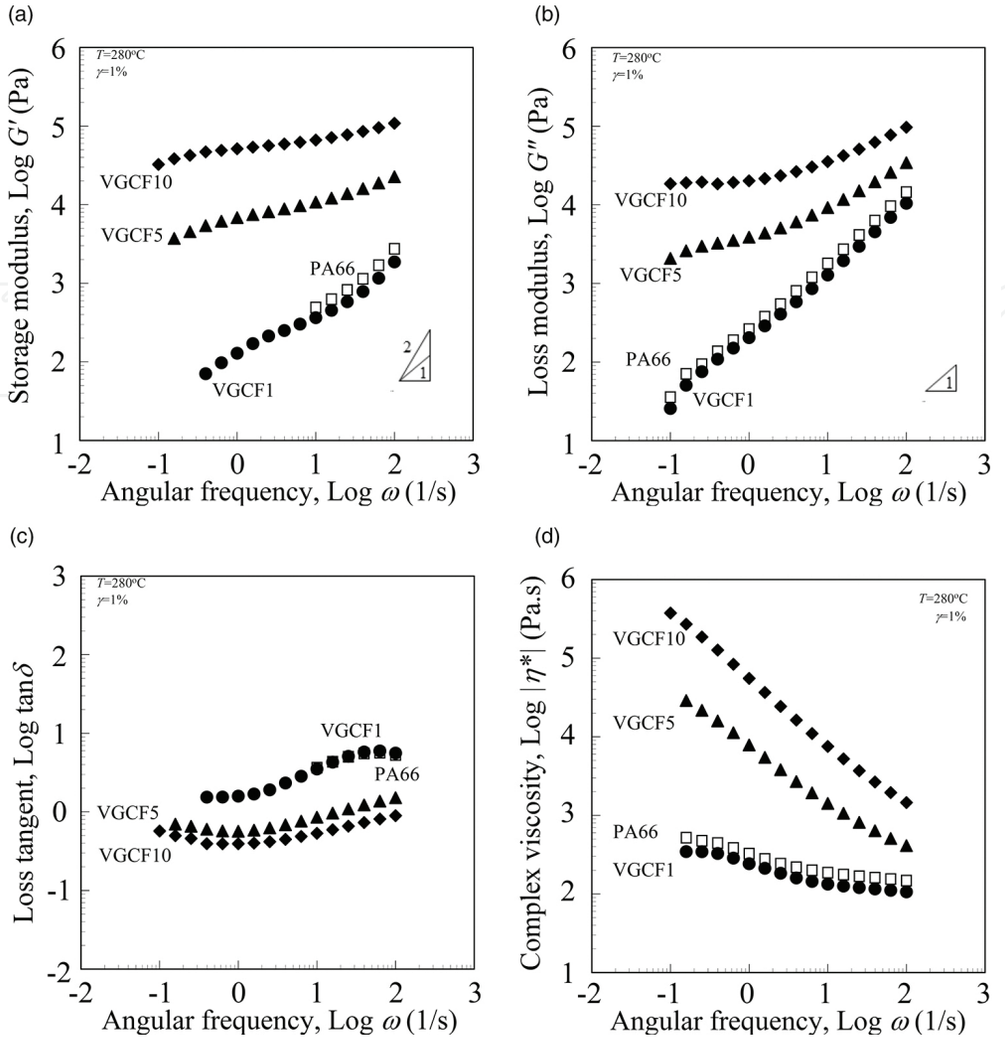

Figure 4. Dynamic viscoelastic properties as a function of angular frequency for VGCF/PA66 composites at 1% strain and 280°C. (a) Storage modulus. (b) Loss modulus. (c) Loss tangent. (d) Complex viscosity.

in high ω region is as small as 0.95. The G' of neat PA66 is generally proportional to ω^2 (log $G' \propto \log \omega^2$) in the linear dynamic viscoelastic models [41, 42]. Thus, the slope of G' against ω is 2, which is log $G' \propto 2\log \omega$, although that of neat PA66 used in this study has a different tendency. This may be attributed to the material properties of PA66 used such as molecular structure, molecular weight distribution, orientation, etc., although the reason is not clear because the G' of neat PA66 in low ω region is not measured because it is below the detection limit of the G' measured using this apparatus. On the other hand, the G' of VGCF/PA66 composites has a different behavior according to the volume fraction of VGCF V_f. That of VGCF1 has the same tendency as that of neat PA66; however, that of VGCF is slightly small than that of neat PA66 in the whole range of ω. The slope of G' against ω of VGCF1 in low and high ω region becomes higher than that of VGCF1 in the middle ω region. Moreover, G' of VGCF5 and VGCF10 is remarkably higher than that of PA66, and VGCF 5 and VGCF10 show the typical G' of highly filled systems [42, 43], although V_f in the composites is only 5 vol%.

The slopes of G' against ω become small, indicating the "second rubbery plateau," i.e., the long-scale relaxation time [25, 41, 42]. Hence, the viscoelastic properties of VGCF/PA66 composites change from liquid-like (viscous behavior) to solid-like (elastic behavior) according to V_f. This second rubbery plateau behavior suggests the presence of an apparent yield stress, which can be attributed to the strong fiber network formed due to the size of VGCF. This is in accordance with theoretical expectations and experimental observations for highly filled systems [43–47]. Similar phenomena have been reported by other systems [25, 31–33].

Code	Slope of G'-ω		Slope of G''-ω	
	Low ω	High ω	Low ω	High ω
PA66	-	0.95	1.05	0.90
VGCF1	0.65	0.94	1.17	0.91
VGCF5	0.41	0.38	0.39	0.61
VGCF10	0.22	0.26	0.05	0.48

Table 1. Slope of viscoelastic properties as function of angular frequency curves of VGCF/PA66 composites in low and high frequencies.

On the contrary, the loss modulus G'' in **Figure 4(b)** has the same tendency as G'. The G'' of VGCF1 is slightly smaller than that of neat PA66. The slope of G'' against ω of VGCF1 is also about 1, which agrees with the linear viscoelastic model that the slope of G'' is proportional to ω ($\log G'' \propto \log \omega$). On the other hand, the G'' of VGCF5 and VGCF10 is higher than the G'' of neat PA66 in the whole ω region, and the slope of G'' against ω becomes small in low ω regions. However, there is a tendency of G'' being smaller than that of G' since the G' is a more sensitive viscoelastic function to the structural changes of the composites than G'' [20]. From the results of loss tangent tan δ against ω in **Figure 4(c)**, tan δ of VGCF1 is similar to that of neat PA66 (100%), and have a maximum peak in high ω region. The values of tan δ for neat PA66 and VGCF1 are higher than 1 in the whole ω region ($\tan \delta > 1$). This indicates that PA66 and VGCF1 behave like liquid, which is a viscosity-dominant property. In contrast, VGCF5 and VGCF10 have different tendencies, and the values of tan δ for VGCF5 and VGCF10 are smaller than 1 ($\tan \delta < 1$) except that of VGCF5 in high ω regions. Thus, VGCF5 and VGCF10 behave like solid materials, which is an elastic-dominant property. Complex viscosity $|\eta^*|$ in **Figure 4(d)** shows the different tendencies according to the V_f. $|\eta^*|$ of neat PA66 and VGCF1 slightly decreases with increasing V_f. In addition, their smaller value than neat PA66 in the whole ω region is a very interesting behavior. On the other hand, the $|\eta^*|$ of VGCF5 and VGCF10 abruptly decreases with increasing ω, which exhibits a very strong shear thinning effect. The curves of $|\eta^*|$ versus ω have a slope of -45°. This behavior indicates the presence of an apparent yield stress in low ω regions. Furthermore, the curve of $|\eta^*|$ versus ω of VGCF1 is remarkably different from that of VGCF5 in low ω regions. This may be attributed to the changes in the fiber network formation. This tendency thus indicates the presence of the transition point of the internal structure, that is, the rheological percolation threshold, which is almost equal to the gel transition point from liquid-like to solid-like behavior.

http://dx.doi.org/10.5772/64531

2.5. Influence of volume fraction

The influence of volume fraction of VGCF V_f on the rheological properties of VGCF/PA66 composites is discussed here. The relative complex viscosity $|\eta^*|_r$ is plotted against volume fraction of VGCF V_f in **Figure 5**. Here, the relative value is given by the values of VGCF/PA66 composites with various V_f divided by that of neat PA66. Three types of angular frequencies: ω = 0.25, 2.5, and 25 rad/s were used as a parameter. The $|\eta^*|_r$ of VGCF/PA66 composites at various ω has a minimum peak at 1 vol%. It then rapidly increases with increasing V_f, and it seems to be remarkably influenced by ω. These results may be attributed to the internal microstructure due to the interaction between fiber and polymer matrix. Especially, the particular phenomena of the complex viscosity of the composites with low fiber content (V_f= 1 vol%), which are smaller than those of neat PA66, are observed in this study. Similar phenomena have been reported by other systems [15, 19, 20, 36]. These phenomena may be due to the self-lubrication of VGCF and also due to the two dimensionally oriented fiber structure formation, which has the possibility to reduce the viscoelastic properties of the composites less than that of matrix polymer. However, it is difficult to confirm these reasons in the present situation. Furthermore, VGCF/PA66 composites sharply increase with V_f between 1 and 5 vol%. This critical composition is regarded as a rheological percolation. At high fiber content, the fiber-fiber interaction is more pronounced. Thus, these results demonstrate that fiber size parameters such as diameter, length, and aspect ratio have strong influence on the viscoelastic properties of VGCF/PA66 composites.

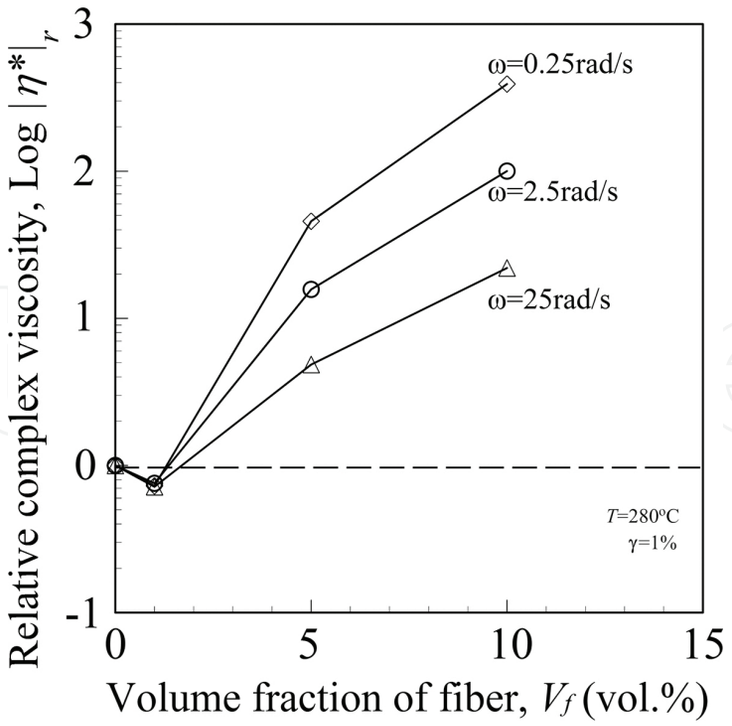

Figure 5. Influence of volume fraction of fiber on relative complex viscosity for VGCF/PA66 composites at 1% strain and 280°C.

2.6. Relationship between storage modulus and loss modulus

The relationship between storage modulus and loss modulus at 1% strain of VGCF/PA66 composites is shown in **Figure 6**. This log G' versus log G'' plots are called as "Han plot" or "modified Cole-Cole plot" [33, 46, 48], which is an analogous Cole-Cole plot used in dielectric spectroscopy. Such plot was used by Han et al. [33] to investigate temperature-induced changes in the microstructure of homopolymers, block copolymers, and polymer blends, and by Potschke et al. [46] to indicate the change of the microstructure in CNT-filled polymer composites such as CNT/PC nanocomposites. It was proposed that the shift and change in the slope of the log G' versus log G'' curves indicate that the microstructure changes significantly with addition of CNT. The curves of various VGCF/PA66 composites in this study show the different behavior related to V_f. The neat PA66 and VGCF1 draw the same curves, and G' is smaller than G'', which means the viscoelastic properties are dominated by the viscous properties. On the other hand, G' at a given G'' of VGCF5 and VGCF10 increases significantly with increasing V_f. Thus, the slope of G' versus G'' decreases with increasing V_f. In addition, the curves of a part of VGCF5 and the whole VGCF10 are located higher than the broken line in **Figure 6**, which contributes to a more dominant role for the elastic properties than the viscous ones. Similar behavior has been reported by other carbon nanotube-filled polymer composites such as CNT/PC [46], CNT/PLA [49], etc. Also, Potschke et al. [46] and Kitano et al. [44] found a similar response of first normal stress difference versus shear stress for glass-fiber-filled polyethylene melts under steady shear conditions. In this study, VGCF clearly present fiber content dependence, confirming the presence of strong interactions between fiber and polymer matrix caused by the nanoscale fiber size such as fiber diameter. Moreover, the decrease of the slope with the increase of fiber content indicates that composites become more heterogeneous due to increasing the interactions between fiber and fiber. It is found from these results that VGCF/PA66 composites change the microstructure according to the fiber content.

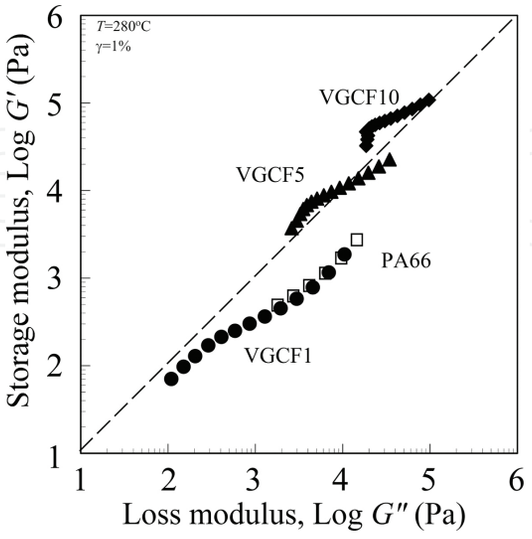

Figure 6. Relationship between storage modulus and loss modulus for VGCF/PA66 composites for VGCF/PA66 composites at 1% strain and 280°C.

http://dx.doi.org/10.5772/64531

2.7. Complex modulus dependences

The influence of complex modulus on the viscoelastic properties of VGCF/PA66 composites is discussed in this section in order to clarify the apparent yield stress and the rheological percolation behavior. A long-scale relaxation time was observed by the curves of G'–ω of VGCF/PA66 in the long-scale time region (in low ω regions) as mentioned earlier. This may be due to the fiber network formation in the composites, indicating the presence of an apparent yield stress in low ω regions. The apparent yield value of $|G^*|$ is thought to be a critical value which determines whether material can flow or not. To discuss this apparent yield stress, the complex viscosity $|\eta^*|$ is plotted against complex modulus $|G^*|$ in double logarithmic coordinates for VGCF/PA66 composites as shown in **Figure 7**. In general, the curves of $|\eta^*|$ versus $|G^*|$ show the following behavior: in the case of Newtonian fluids, although $|\eta^*|$ slightly increases with decreasing $|G^*|$, $|\eta^*|$ has a constant value behavior. On the contrary, in non-Newtonian fluids, such as highly filled polymer systems, $|\eta^*|$ does not have the constant value behavior, and $|\eta^*|$ dramatically increases with slightly decreasing $|G^*|$. In particular, the $|\eta^*|$ of high fiber content samples is almost independent of $|G^*|$. This dramatic behavior in which the $|G^*|$ of high fiber content samples decreases gradually in high ω regions may be due to the remarkable change in the structure of VGCF in high ω regions. It can be estimated from $|\eta^*|$ versus $|G^*|$ curves in the low ω region that there are apparent yield values [25]. In this study, $|\eta^*|$ of neat PA66 and VGCF1 gradually increases with decreasing $|G^*|$, which indicates that there is no apparent yield stress. However, the $|\eta^*|$ of VGCF5 and VGCF10 increases rapidly with a slight decrease in $|G^*|$, which shows that there are the yield values. The yield values $|G^*|_y$ of VGCF5 and VGCF10 are 30 and 300 kPa, respectively. Thus, $|G^*|_y$ is strongly dependent on the fiber content. This behavior was reported by other fiber-filled polymer composites and nanocomposites, such as GF/PP [25, 50], organic fiber/PP [42], CNT/UPR [51], etc. In addition, these curves of $|\eta^*|$ versus $|G^*|$ of VGCF/PA66 composites sharply increase with V_f between 1 and 5 vol%, indicating the presence of the rheological percolation threshold. From these results, the internal structure, changes, and yield stress can be estimated from the curves of $|\eta^*|$ versus $|G^*|$.

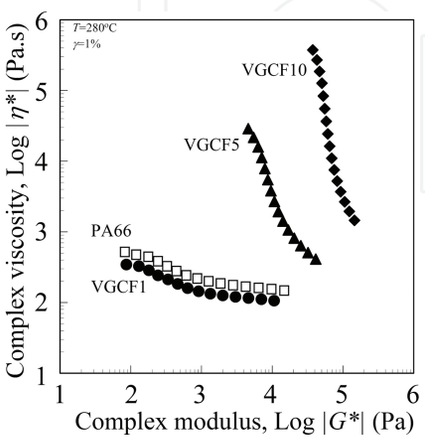

Figure 7. Relationship between complex viscosity and complex modulus for VGCF/PA66 composites at 1% strain and 280°C.

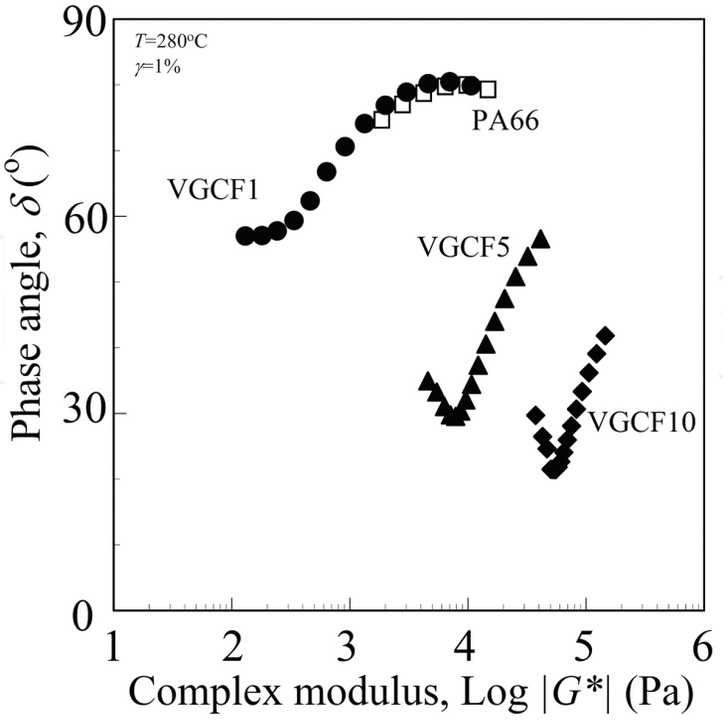

Figure 8. Phase angle versus absolute value of the complex modulus plots (van Gurp-Palmen plot) for VGCF/PA66 composites at 1% strain and 280°C.

On the other hand, the internal structure of the composites and their changes can be identified by van Gurp-Palmen plot [52]. This plot is drawing attention recently as another means of representing the internal microstructures and their change. This plot is considered to be a sensitive indicator for the time-temperature superposition, the presence of long chain branch of the polymer, the polymer entanglement, the gelation behavior, rheological percolation of the polymer nanocomposites, etc. [46, 52–55]. This is due to the emphasis on the change in rheological properties in this δ-|G^*| plot, which are particularly difficult to understand in terms of angular frequency dependence (G'– ω, G''– ω, tan δ – ω curves, etc.). **Figure 8** shows that the phase angle δ (= arctan G''/G') is plotted against the absolute value of the complex modulus |G^*| of VGCF/PA66 composites. The δ-|G^*| curves of neat PA66 and VGCF1 show the same tendency, where δ of neat PA66 and VGCF1 is relatively higher than that of other composites although δ decreases gradually with decreasing |G^*|. However, δ of VGCF5 and VGCF10 decreases abruptly with a slight decrease in |G^*|, and the δ-|G^*| curves of VGCF5 and VGCF10 demonstrate minimum peak behaviors. It is usually assumed that the change in rheological properties near the percolation threshold of a filler network embedded in a viscoelastic liquid is equivalent to the so-called "liquid-solid transition" (or gelation behavior) [47]. It is well known that the gelation point is to plot the loss tangent (tan δ) versus the ω. At gelation point, tan δ is frequency independent. On the other hand, the curve of δ-|G^*| corresponds to a plateau in low complex modulus in this van Gurp-Palmen plot. Previous researches have suggested the following phenomenon in polymer nanocomposites such as CNT-filled polymer systems [46, 47, 53]: In liquid-like behavior, the δ-|G*| curve approaches 90° at the low complex modulus |G^*|, where in solid-like behavior, the δ-|G^*| curves ap-

proaches 0° at the low complex modulus $|G^*|$. However, in the case of VGCF/PA66 composites in this study, the δ-$|G^*|$ curves of neat PA66 and VGCF1 not only demonstrate liquid-like behavior but also solid-like ones at low complex modulus. Furthermore, the δ-$|G^*|$ curves of VGCF/PA66 composites demonstrate remarkable solid-like behavior with increasing V_f. The $|G^*|_{d\text{-min}}$, which is a plateau modulus, is determined by the complex modulus of minimum value of δ in δ-$|G^*|$ curves [56]. The influence of volume fraction of VGCF on the $|G^*|_{d\text{-min}}$ of VGCF/PA66 composites is shown in **Figure 9**. As seen in **Figure 9**, $|G^*|_{d\text{-min}}$ of VGCF/PA66 composites increases sharply with increasing V_f, and exhibits a straight relations between $|G^*|_{d\text{-min}}$ and V_f on this log-log plot. The slope of $|G^*|_{d\text{-min}}$ versus V_f on log-log plot is found to be 2.61 ($|G^*|_{d\text{-min}} \propto V_f^{2.61}$) from the relation in **Figure 9**. Thus, this δ-$|G^*|$ plot may be able to serve as an indicator for the rheological percolation.

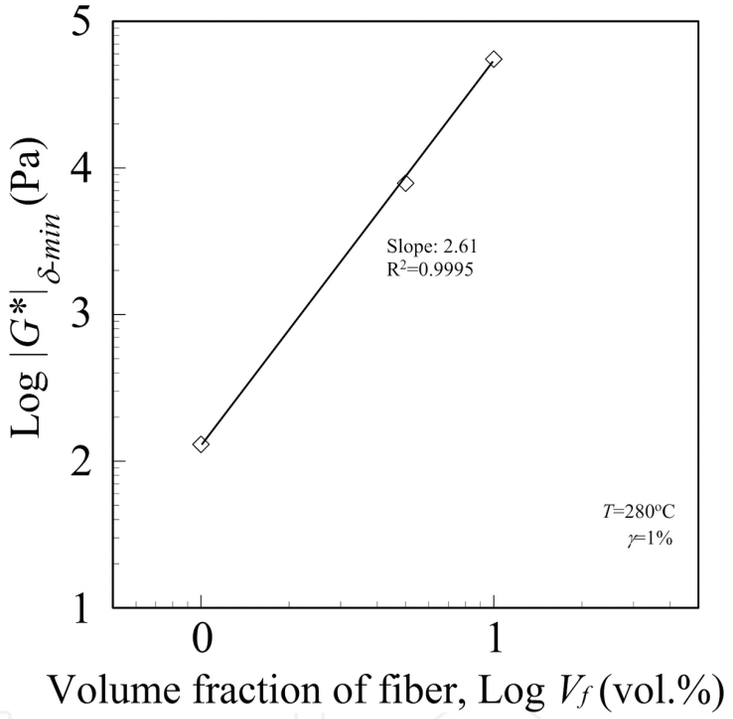

Figure 9. Influence of volume fraction of fiber on absolute value of complex modulus at minimum phase angle for VGCF/PA66 composites at 1% strain and 280°C.

2.8. Temperature dependences

The influence of temperature on the viscoelastic properties of VGCF/PA66 composites is discussed here. The complex viscosity $|\eta^*|$ of VGCF/PA66 composites is plotted against the reciprocal of the absolute temperature $1/T$ at the angular frequency ω of 100 rad/s and at temperatures 270, 280, and 290°C in **Figure 10**. The influence of temperature on $|\eta^*|$ of VGCF/PA66 composites shows the same tendency although the slope of $|\eta^*|$ versus $1/T$ plots slightly differ for each V_f. Especially, the value of VGCF1 is the smallest in this plot in the whole temperature range. From the slope of $|\eta^*|$ versus $1/T$ plots, the apparent activation energy E_a for flow can be calculated from the following Andrade's equation:

$$\eta = A\exp\left(\frac{E_a}{RT}\right) \tag{1}$$

where A is the constant value, R is the gas constant, and η was replaced by $|\eta^*|$ [42, 56]. The apparent activation energy E_a of VGCF/PA66 composites is listed in **Table 2**. E_a is not a constant value for filled systems, but dependent on the volume fraction of fiber [42]. However, it was found that E_a of VGCF/PA66 composites have a complex behavior according to V_f and E_a increases in the following order: VGCF5 < neat PA66 < VGCF10 < VGCF1. It can be said that the fluidity of the materials increases with increasing E_a. In short, VGCF1 with the highest value of E_a indicate high sensitivity to temperature change. In general, it is well known that the increase of V_f decreases the fluidity of the composites due to the formation of the fiber network such as the interaction between fiber and fiber. However, E_a in this study shows the different behavior. This may be attributed to the change in these internal structures at high angular frequency of 100 rad/s.

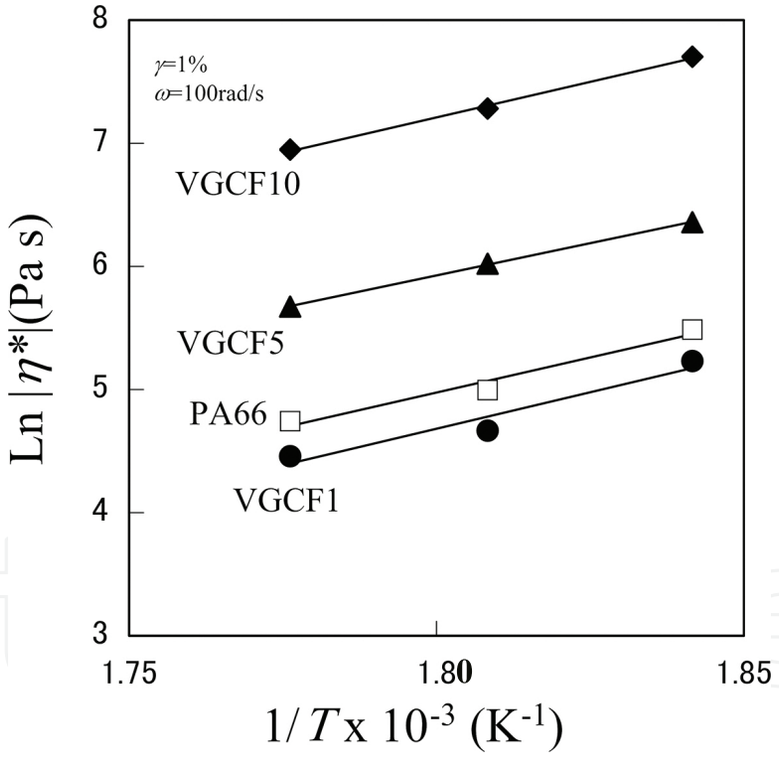

Figure 10. Temperature dependences of complex viscosity for VGCF/PA66 composites at the angular frequency of 100 rad/s and 1% strain. (a) VGCF/PA6/SEBS. (b) VGCF/PA6/SEBS-g-MA.

Code	PA66	VGCF1	VGCF5	VGCF10
E_a (kJ/mol)	94.7	98.5	87.1	95.9

Table 2. Apparent activation energy of flow for VGCF/PA66 composites.

http://dx.doi.org/10.5772/64531

3. Effect of addition of thermoplastic elastomer on dynamic viscoelastic properties of carbon nanofiber-filled polyamide 6 composites in molten state

3.1. Introduction

Recently, there has been considerable discussion on engineering materials containing of nanosized filler such as CNF, CNT, Clay, etc. filled polymer composites based on the multicomponent polymer systems such as binary and ternary polymer blends [18, 22, 31, 32], because they can improve various physical properties with sufficient balances between mechanical and tribological properties by controlling the internal structure such as phase structure and filler dispersion. In our previous works, we considered the relationship between the structural and physical properties of filled polymer composites based on the multicomponent polymer systems required for constructing the technology of internal structures control and investigated the rheological, mechanical, and tribological properties of VGCF-filled polymer blends of PBT and TPE [17, 18], clay-filled polymer blends of PA and TPE [31, 32], etc. It was found that the rheological, mechanical, and tribological properties are improved by the addition of third components such as TPE, PP, PE, etc. However, the rheological properties of filled polymer composites based on the multicomponent polymer systems, in particular, their relationship between rheological properties and internal structure, are yet to be fully clarified. To further enhance the various physical properties, in these CNF-filled polymer composites based on the multicomponent polymer systems, it is very critical to understand the rheological behavior of these multicomponent composites in the molten state such as processability, internal microstructure, changes, and structure-property relationships. The aim of this study is to report the effects of the addition of TPE on the dynamic viscoelastic properties of VGCF/PA6 composites in the molten state. In particular, this study discusses the effects of the addition of TPE, type of TPE, volume fraction of VGCF, strain, and angular frequency on the dynamic viscoelastic properties in the molten state.

3.2. Materials and methods

The materials used in this study were ternary nanocomposites: VGCF-filled polyamide 6 (PA6) composites and the blend of these composites and styrene-ethylene/butylene-styrene copolymer (SEBS), which are called VGCF/PA6/SEBS ternary composites. VGCF (Showa Denko K.K, Japan, d = 150 nm, l = 10 μm) was used as a filler. PA6 (1013B, Ube industries, Ltd., Japan) was used as a matrix polymer. Two types of SEBS: SEBS (standard, Tuftec H1052, Asahi Kasei Chemicals Co., Japan) and SEBS-g-MA (maleic anhydride (MA) grafted SEBS, Tuftec M1943) were used as the blending materials. The content of maleic anhydride (MA) was determined at 10 mg CH_3ONa/g by the titration method. The ratio of styrene to ethylene/butylene in both block copolymer was 20/80 by wt%. Details such as code, manufacturer, etc. are listed in **Table 3**. The composition of PA6 and SEBS (or SEBS-g-MA) was fixed at 80/20 wt%, and three kinds of VGCF volume fraction were selected 0, 1, and 5 vol%. Prior to mixing, VGCF-X, PA6, and SEBS were dried in a vacuum oven at 80°C for 12 h until the moisture level was 0.2%. All the

components were dry blended in a small plastic bottle, and subsequently melted and mixed at 85 rpm and 240°C in a twin screw extruder (TEX-30, Japan Steel Works, Ltd., Japan). After mixing, the extruded strands of these ternary composites were cut into 5 mm long pieces by a pelletizer and were dried again at 80°C for 12 h in the vacuum oven. In addition, 1 mm thick sheets were compression molded at the condition of 240°C, 5 MPa, and 3 min, and cut into ϕ25 mm disk shapes for rheological properties measurements.

Materials	Grade	Manufacturer	Note
PA6	1013B	Ube Industries, Ltd.	-
VGCF	VGCF®	Showa Denko K.K.	Fiber diameter = ϕ150 nm Fiber length = 10 μm
SEBS	Tuftec™ H1052	Asahi Kasei Chemicals Corp.	Styrene/Ethylene-Butylene ratio = 20/80
SEBS-g-MA	Tuftec™ M1943	Asahi Kasei Chemicals Corp.	Maleic anhydride functionalized SEBS Styrene/Ethylene-Butylene ratio =20/80

Table 3. Materials used in this study.

Since the experimental methods such as dynamic viscoelastic properties in the molten state are same as the one in Section 2.2, other than measurement temperature of 240°C and morphology observation method, details are omitted here. To clarify the internal structure of these ternary composites such as the dispersion of SEBS (or SEBS-g-MA) and VGCF in PA6 matrix polymer, the surface of samples fractured cryogenically in liquid nitrogen was observed using scanning electron microscope (SEM, EDX-WET SEM, JSM-6360LA, JEOL Ltd., Japan). The cryogenically fractured surface was etched in toluene for 24 h to remove the dispersed SEBS particles. A quantitative analysis of dispersed SEBS particle size was carried out from several SEM microphotographs using two kinds of image processing software (Adobe Photoshop, Adobe and Image J, NIH). The software used identifies each individual dispersed SEBS particle and evaluates its area A. From these findings, the apparent particle size d was calculated as follows:

$$d = \left(\frac{4A}{\pi} \right)^{\frac{1}{2}} \tag{2}$$

The measured particle size was characterized by evaluating number average diameter d_n, weight average diameter d_w, and volume average diameter d_v from more than 250 particles defined as [32, 57, 58]:

$$d_n = \frac{\sum n_i d_i}{\sum n_i} \tag{3}$$

http://dx.doi.org/10.5772/64531

$$d_w = \frac{\sum n_i d_i^2}{\sum n_i d_i} \tag{4}$$

$$d_v = \frac{\sum n_i d_i^4}{\sum n_i d_i^3} \tag{5}$$

where n_i is the number of dispersed particles having diameter d_i. The ratio of d_w/d_n is an indication of polydispersibility, which is the distribution of dispersed particles.

On the other hand, the fiber length of VGCF and its distribution were measured for samples which had been melted and mixed by an ordinary method: burning off the matrix polymer in a furnace at 550°C for 4 h, wetting fibers in water added with trace surfactant, and spreading them on Al stage (for scanning electron micrographs, SEM). The fiber length distribution of VGCF was observed from SEM. The length of at least 250 fibers was scanned in different regions for evaluating them accurately. A quantitative analysis of the fiber length was made from several micrographs using two kinds of image processing software as mentioned earlier. The number average fiber length l_n and weight average fiber length l_w were calculated according to the following equations [19, 23]:

$$l_{\mathrm{n}} = \frac{\sum N_i l_i}{\sum N_i} \tag{6}$$

$$l_{\mathrm{w}} = \frac{\sum N_i l_i^2}{\sum N_i l_i} \tag{7}$$

where N_i is the number of fibers and l_i is the fiber length. The fiber distribution l_w/l_n was calculated from above equations.

3.3. Strain dependences

The strain dependence of the dynamic viscoelastic properties of ternary composites (VGCF/PA6/SEBS) is discussed here. It was measured by strain sweep testing in order to characterize the transition from linear to nonlinear viscoelastic properties of the ternary composites and also to estimate the change in internal microstructure such as the dispersion and localization of VGCF and SEBS, etc. of these ternary composites. Only the storage modulus G' curves are presented in this study since G' is the more sensitive rheological function to the structural changes of the composites than other functions as mentioned in Section 2.3. The strain dependence of storage modulus G' of ternary composites (VGCF/PA6/SEBS) is shown in **Figure 11(a)** (VGCF/PA6/SEBS composites) and (b) (VGCF/PA6/SEBS-g-MA composites), respectively. This measurement was carried out for all samples of temperature at 240°C and

the angular frequency at 3.5 rad/s. The strain dependences of G' show remarkably different behavior according to the type of material such as V_f, with or without SEBS and type of SEBS. G' of neat PA6 exhibits a linear behavior, in which the modulus is a constant over a wide range of strain amplitude γ. The G' of VGCF1/PA66 binary composites has the same tendency as neat PA6, and is slightly higher than that of neat PA6. On the other hand, G' of PA6/SEBS binary blends and VGCF1/PA6/SEBS ternary composites shows the same linear behaviors as neat PA6; however, it is higher than that of VGCF1/PA6 composites. On the contrary, the G' of VGCF5/PA6 composites and VGCF5/PA6/SEBS ternary composites shows the linear plateau only in low strain regions, and rapidly decreases with increasing γ, which are independent transition from linear to nonlinear behavior. The G' of VGCF5/PA6/SEBS ternary composites is higher than that of VGCF5/PA6 composites, and the magnitude of the increase is almost 1 digit (decade) on the log scale. On the other hand, the G' of SEBS-g-MA systems, which are PA6/SEBS-g-MA and VGCF/PA6/SEBS-g-MA, shows a different behavior from the SEBS systems. G' of PA6/SEBS-g-MA shows a linear behavior in wide strain region until several 10%, and is higher than that of PA6/SEBS blends. The G' of VGCF1/PA6/SEBS-g-MA and VGCF5/PA6/SEBS-g-MA has the same tendency as that of PA6/SEBS, and their values, which are the plateau modulus G'_p, increase with increasing V_f. It was found from these results that G'-γ curves are changed by material composition factors such as the addition of VGCF and SEBS, volume fraction of fiber V_f, and type of SEBS, which is SEBS and SEBS-g-MA. In addition, these phenomena are distinguished as the following mechanisms: the addition and volume fraction of VGCF emphasize the nonlinear behavior and increase the plateau modulus. The addition of SEBS increases the magnitude value of the plateau modulus. Especially, the type of SEBS changes the magnitude value of the plateau modulus and the critical strain value, which is the transition point from linear to nonlinear viscoelastic behavior. These may be attributed to the changes in the internal microstructure formation of the composites, which is the dispersion of VGCF and SEBS, interaction between fiber and matrix polymer, localization, size of dispersed SEBS particles and VGCF, agglomerations of VGCF, interaction between fiber and fiber, etc.

To further clarify the transition point from linear to nonlinear behavior, the relationship between critical strain value γ_c and volume fraction of fiber V_f of VGCF/PA6, VGCF/PA6/SEBS, and VGCF/PA6/SEBS-g-MA composites at 3.5 rad/s and 280°C is shown in **Figure 12** in the semilogarithmic scale. Here, the critical strain value γ_c can be calculated from the curves of the relative storage modulus G'_r (= G'/G'_p) – strain γ of these composites using the method in Section 2.3. γ_c of various VGCF/PA6 composites abruptly decreases with increasing V_f and exhibits a straight relations between γ_c and V_f in the semilogarithmic plot. The slope of the γ_c - V_f plot gradually increases in the following order: VGCF/PA6 (–9.95) < VGCF/PA6/SEBS (–6.50) < VGCF/PA6/SEBS-g-MA (–3.24). It was found from these results that material composition factors such as the addition of VGCF and SEBS, volume fraction of fiber V_f, and type of SEBS, which is SEBS and SEBS-g-MA, have strong influences on the strain dependence of viscoelastic properties. In particular, the strain dependences of ternary composites have the different behavior because of these factors. These behaviors may be considered to be due to the change in the internal structure of the composites as mentioned earlier.

http://dx.doi.org/10.5772/64531

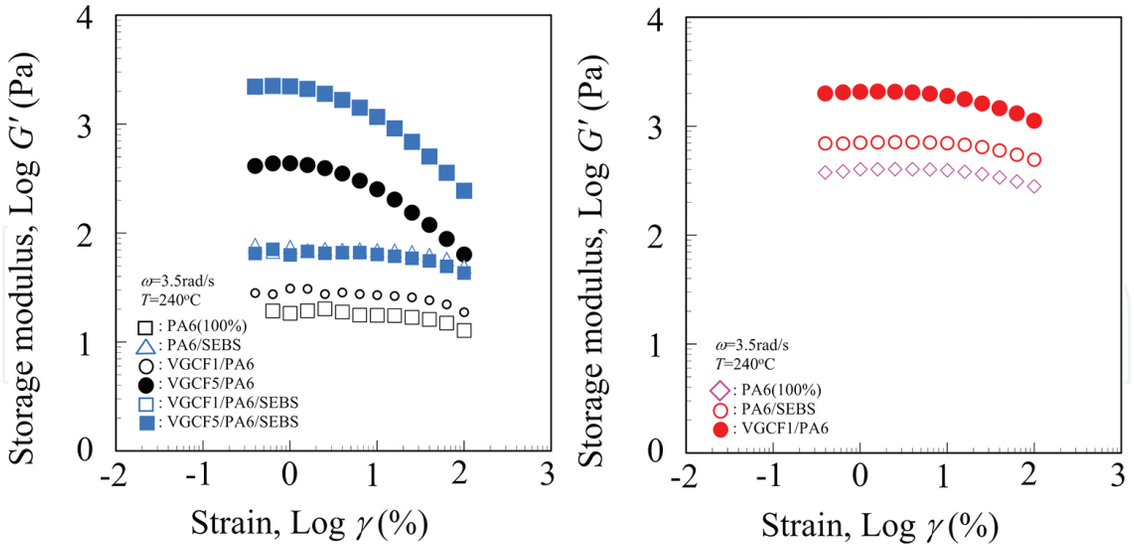

Figure 11. Storage modulus as a function of strain for ternary composites (VGCF/PA6/SEBS) at 3.5rad/s and 240°C. (a) VGCF/PA6/SEBS. (b) VGCF/PA6/SEBS-g-MA.

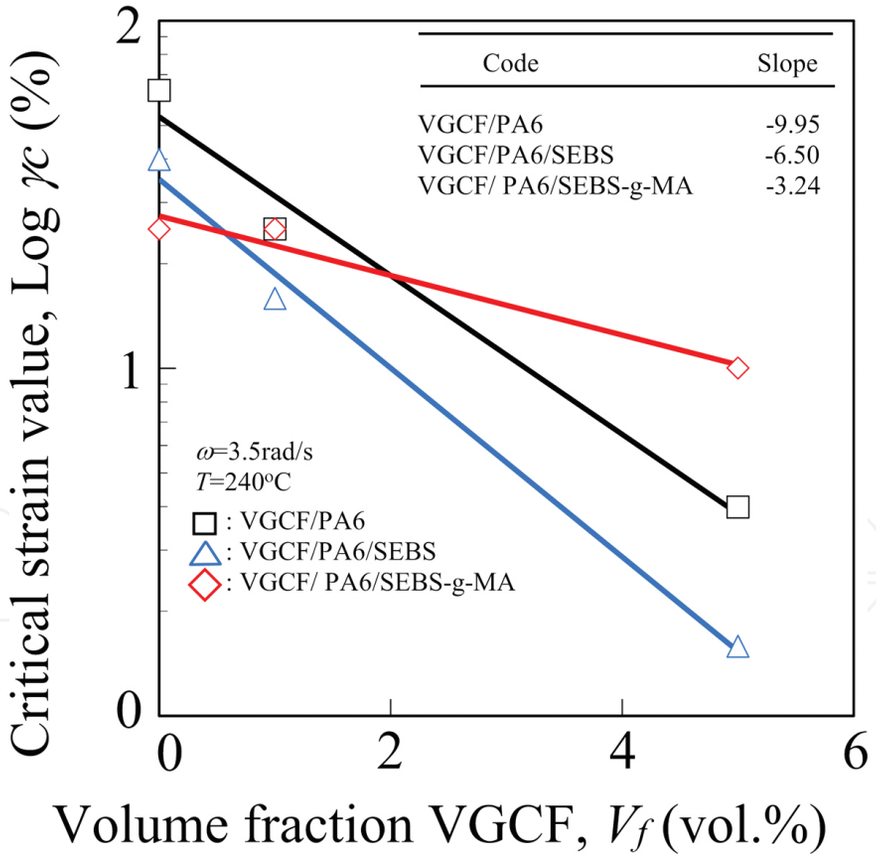

Figure 12. The dependence of critical strain on volume fraction of VGCF for ternary composites (VGCF/PA6/SEBS) at 3.5rad/s and 240°C.

3.4. Angular frequency dependences

The influence of these materials composition factors on the dynamic viscoelastic properties of ternary composites (VGCF/PA6/SEBS) in the molten state is discussed in this section. These properties are strongly dependent on the internal microstructure formation of the polymer composites. We shall discuss the angular frequency dependence, which is the basic variable in these properties. The dynamic viscoelastic properties of these ternary composites are plotted as a function of ω at temperature 240°C and strain 1% in **Figure 13(a)** (storage modulus G', V_f= 1 vol%), **(b)** (loss modulus G'', V_f= 1 vol%), **(c)** (storage modulus G', V_f= 5 vol%), and **(d)** (loss modulus G'', V_f= 5 vol%), respectively. In **Figure 13(a)**, the slopes of G' and G'' against ω in the low and high ω regions are listed in **Table 4**. The G' of neat PA6 increases with increasing ω, disagreeing with the linear viscoelastic model [41, 42]. The slope of G'- ω in high ω regions of neat PA6 is 1.57. The G' of VGCF1 shows the same tendency as that of neat PA6, and is slightly higher than that of neat PA6. PA6/SEBS blends show the typical G' of the multicomponent systems [31, 32]. The slope of G' against ω, in particular, in low ω regions becomes small with the addition of SEBS, indicating the "second rubbery plateau," i.e., the long scale relaxation time [25, 41, 42]. This may be attributed to the heterogeneous structure such as sea-island structures in PA6/SEBS blends. G' of VGCF1/PA6/SEBS composites is higher than that of PA6/SEBS blends, which shifts toward high elasticity (solid-like) with the addition of VGCF caused by the changes in the internal structures such as interaction between fibers or agglomerations. Furthermore, the G' of PA6/SEBS-g-MA blends and VGCF1/PA6/SEBS-g-MA composites is much higher than that of PA6/SEBS blends and VGCF1/PA6/SEBS composites, and the slopes of G' against ω of these SEBS-g-MA systems are visible in low ω regions, indicating the formation of small dispersed phase and the new structure in these polymer blends and composites. In **Figure 13(b)**, loss modulus G'' of these ternary composites shows a slightly different behavior from the G'. The values of G'' of these materials in low ω regions increase in the following orders: PA6 < VGCF/PA6 < PA6/SEBS < VGCF1/PA6/SEBS < PA6/SEBS-g-MA < VGCF1/PA6/SEBS-g-MA composites, although those of these materials in high ω regions have different behaviors: PA6 < PA6/SEBS < VGCF/PA6 < VGCF1/PA6/SEBS < PA6/SEBS-g-MA < VGCF1/PA6/SEBS-g-MA composites. In general, storage and loss moduli in low ω regions are dominated by the internal structure, and those in high ω regions dominated by the polymer matrix. However, the little reverse phenomenon can be explained in the present stage. On the other hand, in **Figure 13(c)** and **(d)** with VGCF 5 vol% loading systems, the G' of various composites shows remarkably the typical storage and loss moduli of highly filled systems, indicating the "second rubbery plateau." However, another behavior, which is crossover of VGCF5/PA6/SEBS and VGCF5/PA6/SEBS-g-MA composites, is clearly seen at ω = 1–10 rad/s. In particular, in low ω regions, the G' and G'' of VGCF5/PA6/SEBS composites are higher than those of VGCF5/PA6/SEBS-g-MA composites. In short, VGCF5/PA6/SEBS composites demonstrate solid-like behavior. These behaviors may be explained by the changes in the internal structure caused by the dispersed phases, the interaction between fiber and polymer matrix, the interaction between fibers, agglomerations, etc. Therefore, it is necessary to understand these behaviors to observe the morphology of ternary composites (VGCF/PA6/SEBS). From the results of the angular frequency dependences of storage and loss moduli of ternary composites mentioned above, these dependences show different behaviors according to the

http://dx.doi.org/10.5772/64531

addition of VGCF and SEBS, type of SEBS, and volume fraction of fiber. The addition of SEBS was changed by the tendency of G' and G'' – ω curves, which shows remarkably the "second rubbery plateau" in low ω regions. In particular, these dependences appear to be conspicuously high for the composites with SEBS-g-MA, except for only VGCF5/PA6/SEBS composites in low ω regions. On the other hand, the addition of VGCF and volume fraction of fiber slightly enhanced these dependences.

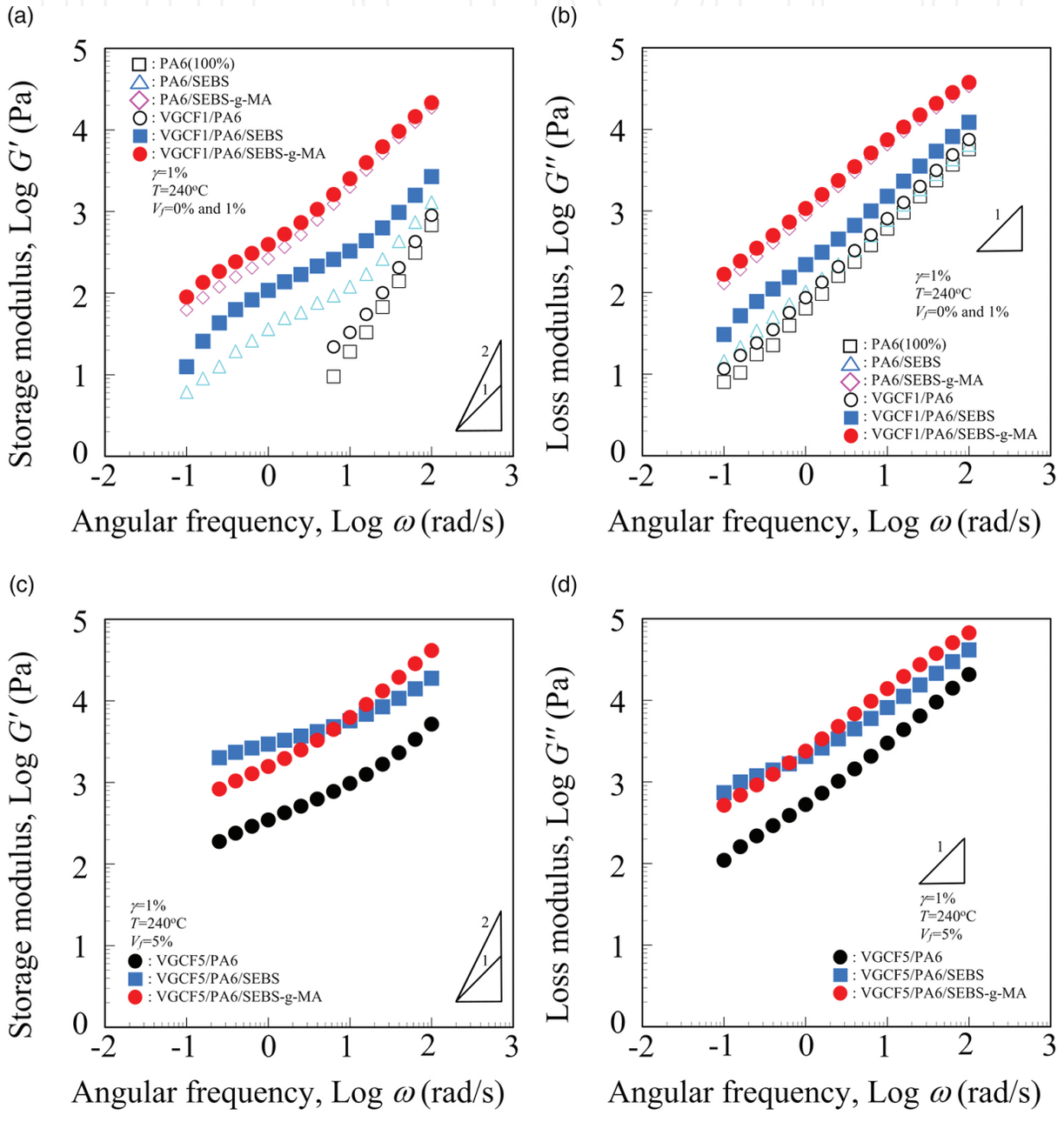

Figure 13. Dynamic viscoelastic properties as a function of angular frequency for ternary composites (VGCF/PA6/SEBS) composites at 1% strain and 240°C. (a) Storage modulus (V_f=0% and 1%). (b) Loss modulus (V_f=0% and 1%). (c) Storage modulus (V_f=5%). (d) Loss modulus (V_f=5%)

Code	Slope of G'-ω		Slope of G''-ω	
	Low ω	High ω	Low ω	High ω
PA6 (100%)	-	1.57	0.91	0.98
PA6/SEBS	0.78	1.04	0.86	0.92
PA6/SEBS-g-MA	0.62	0.97	0.84	0.71
VGCF1/PA6	-	1.45	0.87	0.97
VGCF5/PA6	0.58	0.72	0.67	0.84
VGCF1/PA6/SEBS	0.91	0.92	0.84	0.91
VGCF5/PA6/SEBS	0.44	0.52	0.42	0.71
VGCF1/PA6/SEBS-g-MA	0.63	0.93	0.80	0.70
VGCF5/PA6/SEBS-g-MA	0.56	0.82	0.66	0.69

Table 4. Slope of viscoelastic properties as function of angular frequency curves of ternary composites (VGCF/PA6/SEBS) in low and high frequencies.

3.5. Influence of volume fraction and type of SEBS

The influence of volume fraction of fiber and type of SEBS on the rheological properties of ternary composites (VGCF/PA6/SEBS) is discussed in this section. The relative storage modulus G'_r is plotted against the volume fraction of fiber V_f in **Figure 14(a)** (in low ω regions, ω = 0.25 rad/s) and (b) (in high ω region, ω = 25 rad/s), respectively. Here, this value is given by the value of various ternary composites (VGCF/PA6/SEBS) divided by that of neat PA6. G'_r of all ternary composites (VGCF/PA6/SEBS) increases with increasing V_f. This tendency changes with the type of SEBS and the angular frequency regions. The increase ratios of G'_r

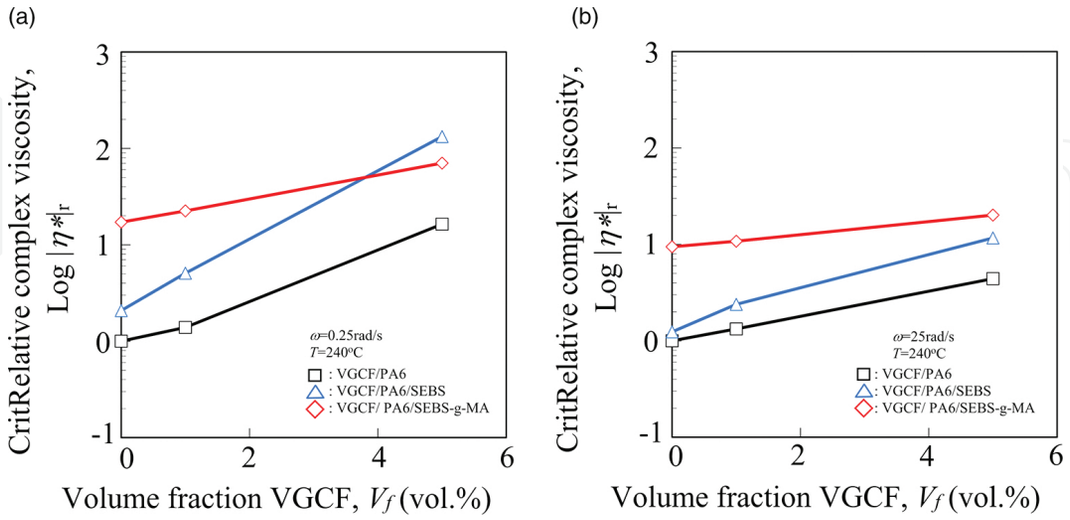

Figure 14. Influence of volume fraction of fiber on relative complex viscosity for ternary composites (VGCF/PA6/SEBS) at 1% strain and 240°C. (a) Relative complex viscosity. (b) Relative complex viscosity.

against V_f in low ω regions (**Figure 14(a)**, ω = 0.25 rad/s) are larger than those in high ω regions (**Figure 14(b)**, ω = 25 rad/s). It should be noted that G'_r of VGCF5/PA6/SEBS composites is higher than that of VGCF5/PA6/SEBS ones. In general, storage modulus in low ω regions is dominated by the internal structure as mentioned earlier. Thus, it is necessary for understanding this behavior to observe the internal structure of these ternary composites, and the morphologies of these composites will be discussed in the next section.

3.6. Morphology

To further clarify the relationship between the dynamic viscoelastic properties and internal structure of ternary composites (VGCF/PA6/SEBS), we discuss the morphologies of these composites, which are the internal structure such as fiber network formation and dispersed SEBS particles. We observed the cryogenically fractured surfaces of various ternary composites, which were etched by toluene in order to remove the dispersed SEBS particles using a scanning electron microscope. **Figure 15** shows the SEM photographs of the etched fracture surfaces of PA6/SEBS blends (**Figure 15(a)**), VGCF1/PA6/SEBS composites (**Figure 15(b)**), VGCF5/PA6/SEBS composites (**Figure 15(c)**), PA6/SEBS-g-MA blends (**Figure 15(d)**), VGCF1/PA6/SEBS-g-MA composites (**Figure 15(e)**), and VGCF5/PA6/SEBS-g-MA composites (**Figure 15(f)**), respectively. Here, **Figure 15(a)-(c)** was observed at the magnification of 5000, and **Figure 15(d)-(f)** was observed at 20,000. Each polymer blends and ternary composite exhibited typical separate spherical phases (dispersed SEBS particles) in PA6 continuous matrix domains. **Table 5** summarizes the various data of the dispersed SEBS particles for each ternary composite, calculated by image processing from SEM photographs such as number average diameter d_n, weight average diameter d_w, volume average diameter d_v, and polydispersibity d_w/d_n. The sizes of dispersed SEBS particles change with the type of SEBS and volume fraction of VGCF, and these decrease in the following orders: PA6/SEBS > VGCF1/PA6/SEBS > VGCF5/PA6/SEBS >> PA6/SEBS-g-MA > VGCF1/PA6/SEBS-g-MA > VGCF5/PA6/SEBS-g-MA composites. This means that the size of dispersed SEBS particles decreases with the SEBS with functional groups of maleic anhydride (MA), and these SEBS particles decrease with increasing V_f. These morphological changes are the consequence of graft reaction between the PA6 matrix and MA in SEBS, which separates spherical particles in continuous matrix domains. MA groups are expected to induce strong interaction and reaction due to high reactive functional groups such as amine and carboxyl end groups and acid amide in the main chain of PA [32]. These observations indicate that dynamic viscoelastic properties shown earlier correlate closely with the size of dispersed SEBS particles. On the other hand, we have to consider the presence of VGCF, which may complicate these behaviors. Each ternary composite shows good dispersion of VGCF, and the location of VGCF is in PA6 continuous matrix domains. For comparison, it was not observed by VGCF in toluene solution for etching in order to remove the SEBS particles. The number average fiber length l_n, weight average fiber length l_w, fiber distribution l_w/l_n, and number average aspect ratio $(a_r)_N$ are listed in **Table 6**. The number average aspect ratio $(a_r)_N$ is defined as l_n/d, where d is the average fiber diameter of VGCF ($d = \phi 150$ nm). The fiber lengths values of l_n, l_w, and $(a_r)_N$ of VGCF/PA6 and VGCF/PA6/SEBS-g-MA decrease with increasing V_f, although those of VGCF/PA6/SEBS

increase with V_f. Fiber distribution l_w/l_n has complex behavior; however, VGCF/PA6/SEBS-g-MA has the highest values in this study. What should be noted is that the fiber length value of VGCF5/PA6/SEBS is much longer than those of other composites except for VGCF1/PA6 composites. These results coincide with the dynamic viscoelastic values earlier, that is, the storage modulus of VGCF5/PA6/SEBS is crossover with that of VGCF5/PA6/SEBS in low ω regions. This may be attributed to the change in internal structure by the interactions of fiber-fiber and fiber-matrix, and agglomerations caused by the increase in fiber length values. Therefore, the internal structure of ternary composites was found to correlate closely with the dynamic viscoelastic properties of ones. In general, it is well known that the fiber length and the aspect ratio of these compounds in the twin screw extruder depend on concentration, characteristics of these compounds, and the addition of third component, which suggests fiber degradation may be due to the interactions between fiber and matrix, and between fibers. However, it is difficult in the present stage to understand the exactly reason why the fiber length of VGCF5/PA6/SEBS are longer than those of other composites in this study.

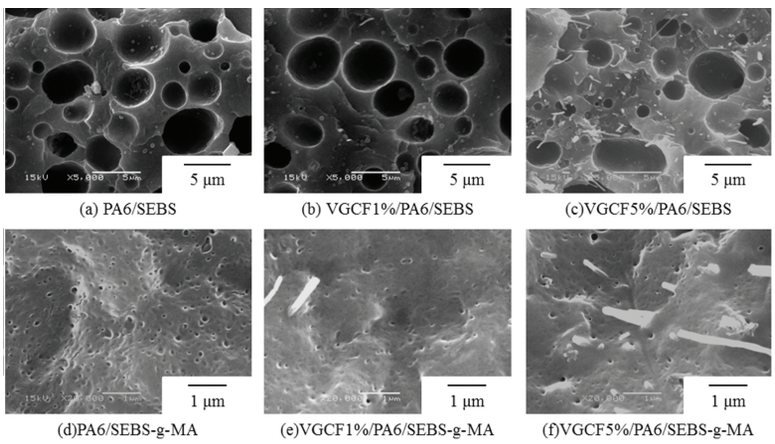

Figure 15. SEM micrographs of etched fracture surface for the ternary composites (VGCF/PA6/SEBS) (SEBS content is 20 wt% and etched with toluene for 24 h to remove the dispersed phases): (a) PA6/SEBS, (b) VGCF 1%/PA6/SEBS, (c) VGCF 5%/PA6/SEBS, (d) PA6/SEBS-g-MA, (e) VGCF 1%/PA6/SEBS-g-MA, and (f) VGCF 5%/PA6/SEBS-g-MA. (a) VGCF fiber length. (b) SEBS particle size.

Material	d_n (nm)	d_w (nm)	d_v (nm)	d_w/d_n
PA6/SEBS	2930	3750	4880	1.28
VGCF1/PA6/SEBS	2810	3920	4940	1.39
VGCF5/PA6/SEBS	2260	3060	4250	1.36
PA6/SEBS-g-MA	88	97	121	1.11
VGCF1/PA6/SEBS-g-MA	81	88	104	1.08
VGCF5/PA6/SEBS-g-MA	51	59	95	1.17

Table 5. Dispersed SEBS particle size of ternary composites (VGCF/PA6/SEBS).

Material	l_n (μm)	l_w (μm)	l_w/l_n	$(a_r)_N$
VGCF1/PA6	3.28	3.64	1.11	21.9
VGCF5/PA6	2.91	3.23	1.11	19.4
VGCF1/PA6/SEBS	2.90	3.12	1.08	19.3
VGCF5/PA6/SEBS	3.04	3.38	1.11	20.3
VGCF1/PA6/SEBS-g-MA	2.28	3.12	1.37	15.2
VGCF5/PA6/SEBS-g-MA	2.22	2.96	1.33	14.8

Table 6. Fiber length, its distribution, and aspect ratio of ternary composites (VGCF/PA6/SEBS).

Furthermore, to clarify the relationships between the morphologies of ternary composites and the dynamic viscoelastic properties of ones, it is necessary to investigate the effect of morphologies of ternary composites on the dynamic viscoelastic properties in detail. G' is replotted as a function of average weight fiber length of VGCF l_w in **Figure 16(a)**, and average weight diameter of dispersed SEBS particles d_w in **Figure 16(b)**, respectively. The fiber length l_w dependence of G' has a complex behavior. It is fundamentally influenced by the volume fraction of fiber and the addition of SEBS rather than the fiber length. In VGCF/PA6/SEBS systems, the longer the fiber length is, the more the increase in G'. On the other hand, the size of diameter of dispersed SEBS particles d_w dependence is not clearly recognized, and G' is strongly influenced by the type of SEBS and the volume fraction of VGCF.

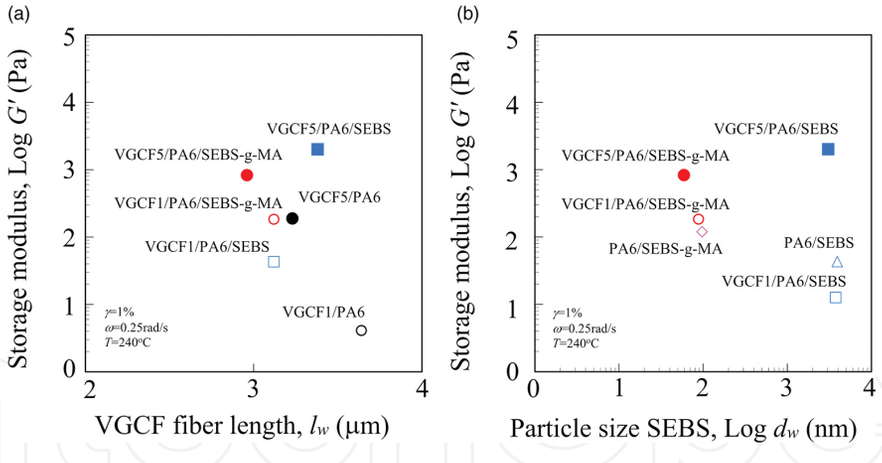

Figure 16. Influence of internal structure parameters such as SEBS particles size and fiber length on storage modulus of ternary composites (VGCF/PA6/SEBS). (a) VGCF fiber length. (b) SEBS particle size.

4. Effect of processing sequence on the dynamic viscoelastic properties of ternary composites (VGCF/PA6/SEBS-g-MA) in molten state

4.1. Introduction

We discussed the dynamic viscoelastic properties of ternary composites (VGCF/PA6/SEBS) in the molten state in the previous section and concluded that the effect of the addition of TPE

on the dynamic viscoelastic properties of VGCF/PA6 composites in the molten state differs according to the viscoelastic value. It was clarified that the dynamic viscoelastic properties of VGCF/PA6/SEBS-g-MA ternary composites are higher than those of VGCF/PA6/SEBS ones. This may be attributed to the change in the internal structure caused by addition of TPE. Thus, it is important to further investigate the relationship between rheological properties and internal structure of these ternary composites. It is well known that the morphologies of these ternary composites are influenced by the processing sequences [34, 35]. Several investigations have been conducted on the effect of processing sequences at melt mixing by twin extruder on the relationship between the morphology and the physical properties of ternary composites such as PA/Clay/SEBS [35, 59], VGCF/PBT/TPE [60], VGCF/PA6/SEBS [22], etc. However, there is not enough information on reliable relations between the internal structure and rheological properties of these ternary composites. The purpose of this study is to report the effect of processing sequences on the dynamic viscoelastic properties of VGCF-filled polymer blends of PA6 and SEBS-g-MA (VGCF/PA6/SEBS-g-MA ternary composites).

4.2. Materials and methods

The materials used in this study were ternary composites (VGCF/PA6/SEBS-g-MA). Since the materials, composition, processing, and experimental methods are the same as in Section 3.2 other than the processing sequence using the twin extruder, they are omitted here. The composition of PA6 and SEBS-g-MA was fixed as 80/20 by weight fraction, and three kinds of VGCF volume fraction were selected as 0, 1, and 5 vol%. All the components were dried for 12 h at 80°C in a vacuum oven beforehand until the moisture level was below 0.2%. Four different processing sequences were carried out: (1) VGCF, PA6 and SEBS-g-MA were mixed simultaneously (process A), (2) VGCF was mixed with PA6 (VGCF/PA6 composites) and then these composites were blended with SEBS-g-MA (process B), (3) SEBS-g-MA was blended with PA6 (PA6/SEBS-g-MA blends) and then these blends were mixed with VGCF (process C), and (4) VGCF were mixed with SEBS-G-MA (VGCF/SEBS-g-MA composites) and blended with PA6 (process D) and then attempted to prepare the ternary composites (VGCF/PA6/SEBS-g-MA). **Figure 17** shows the schematic diagram of four different processing sequences for ternary composites (VGCF/PA6/SEBS-g-MA). The melt of these materials was mixed at 85 rpm and 240°C in a twin screw extruder (TEX-30, Japan Steel Works, Ltd.). After mixing, the extruded strands of these ternary composites were cut in piece of about 5 mm long by a pelletizer and were dried again at 80°C for 12 h in the vacuum oven. In addition, 1 mm thick sheets were compression molded at the condition of 240°C, 5 MPa, and 3 min, and cut into ϕ25 mm disk shapes for rheological properties measurements.

4.3. Angular frequency dependences

The effect of processing sequences on the dynamic viscoelastic properties of ternary composites (VGCF/PA6/SEBS-g-MA) is discussed here. The dynamic viscoelastic properties of these ternary composites with 5 vol% VGCF prepared by various processing sequences are plotted as a function of angular frequency ω in **Figure 18(a)** (storage modulus G') and **(b)** (loss modulus G''), respectively. Each storage and loss moduli increase with increasing ω; however, the

http://dx.doi.org/10.5772/64531

magnitude value of G' and G'', in particular, in low ω regions, changes according to the processing sequences in the following orders: Process A > Process C > Process B = Process D. The decreases of G' and G'' are closely related to the number of mixing of VGCF, and the twice mixing methods of VGCF which remix VGCF such as processes B and C are more effective than unimixing methods such as processes A and C. These may be attributed to the change in the internal structure of these ternary composites by different processing sequences. Another important point is the difference in the order of decrease in G' according to the angular frequency region. In short, the G'- ω curve of process B is crossover to that of processes C and D. This is suggested by the change in the internal structure according to ω. To clarify the effect of processing sequences on G' of these ternary composites, the relative storage modulus G'_r in low ω regions (ω = 0.25 rad/s) is shown in **Figure 19(a)** (V_f= 1 vol%) and **(b)** (V_f = 5 vol%), respectively. Here, this relative value is given by the value of various ternary composites prepared by different processing sequences divided by that of process A. G'_r change according

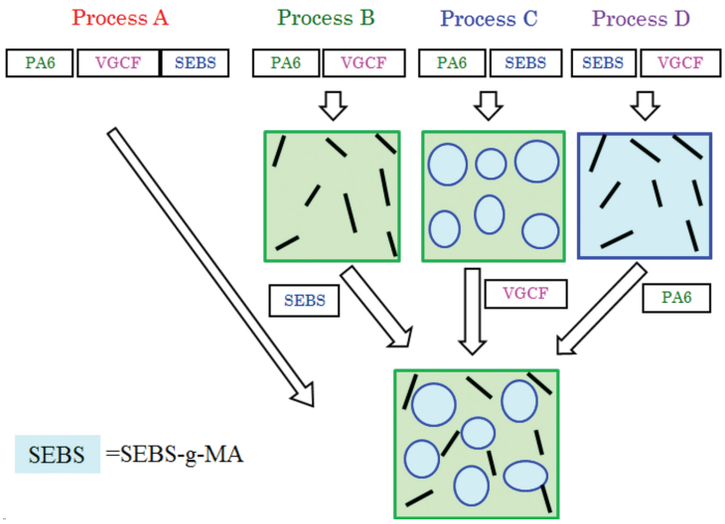

Figure 17. Schematic diagram of four different processing sequences for ternary composites (VGCF/PA6/SEBS-g-MA).

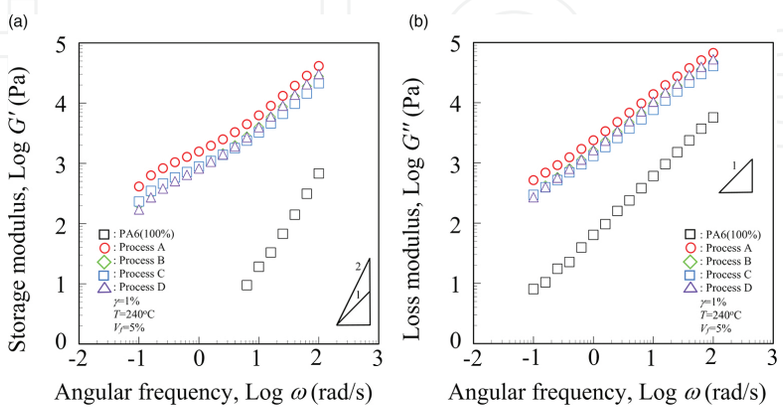

Figure 18. Dynamic viscoelastic properties as a function of angular frequency for various processing sequence of ternary composites (VGCF/PA6/SEBS-g-MA) composites at 1% strain and 240°C. (a) Storage modulus. (b) Loss modulus.

to the processing sequences and the volume fraction of fiber. The G'_r of these various composites with V_f= 1 vol% decreases in the following orders: Process A > Process C > Process D > Process B. On the other hand, that of V_f= 5 vol% decreases in the following orders: Process A > Process C > Process B > Process D. These tendencies may be attributed to the change in the internal structure by the number of mixing as mentioned earlier. However, it is not clearly explained by the order of decrease G'_r changing according to V_f. Therefore, it is necessary to observe the internal structure for better understanding the relationships between processing sequences and dynamic viscoelastic properties of these ternary composites. This will be discussed in the next sections.

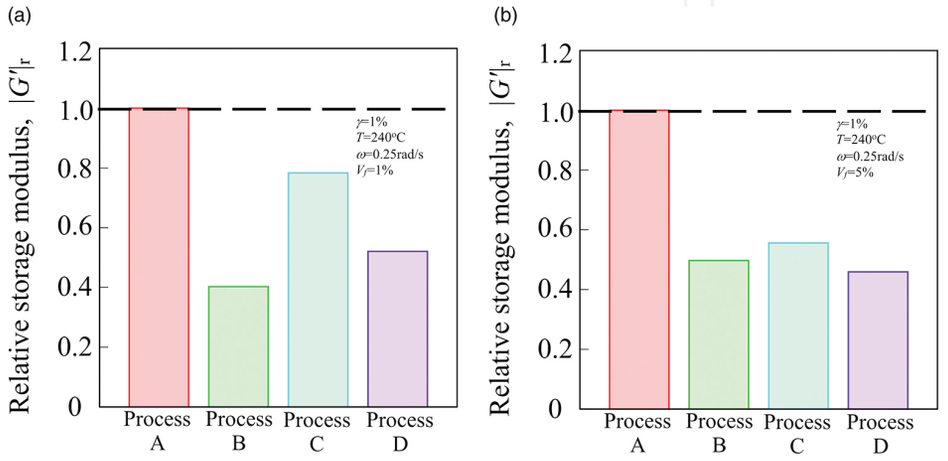

Figure 19. Relative storage modulus for various processing sequence of ternary composites (VGCF/PA6/SEBS-g-MA) composites at 1% strain and 240°C. (a) VGCF 1vol.%. (b) VGCF 5vol.%.

4.4. Morphology

Furthermore, to clarify the relationships between processing sequences and rheological properties of ternary composites (VGCF/PA6/SEBS-g-MA), we observed the internal structure, which is the dispersibility of SEBS particles and VGCF in these ternary composites. **Figure 20** shows the SEM photographs of cryogenically fractured surfaces, which were etched by toluene in order to remove the dispersed SEBS-g-MA particles, of various ternary composites prepared by different processing sequences at the same magnification rate of 20,000. Each ternary composite indicates the good dispersion of VGCF and dispersed SEBS-g-MA particles. In addition, it was not observed for VGCF in toluene solution for etching in order to remove the SEBS particles. Thus, there are VGCFs only in PA6 matrix domains, and are not presented in the dispersed SEBS particle domain. In particular, in the case of process D, VGCF should be present in the SEBS domain; nevertheless, VGCF was mixed with SEBS. However, VGCF was not found in the SEBS domain after mixing the second time in process D. Thus, VGCF is transferred from SEBS domain to the PA6 continuous matrix domain in process D, i.e., the localization of VGCF is changed. The reason for changing the localization of VGCF in process D can be explained by the following mechanisms: VGCF is selected by the PA6 domain, because the viscosity of PA6 is lower than that of SEBS-g-MA at the mixing temperature of

240°C. This is due to the stronger interactions of fiber-matrix polymer, which is wettability and chemical affinity, between VGCF and PA6 than those of VGCF and SEBS-g-MA. In addition, these detail mechanisms, which are filler migration inside a molten heterogeneous medium, were suggested by Fenouillot et al., Elias et al., and Baudouin et al. [61–63].

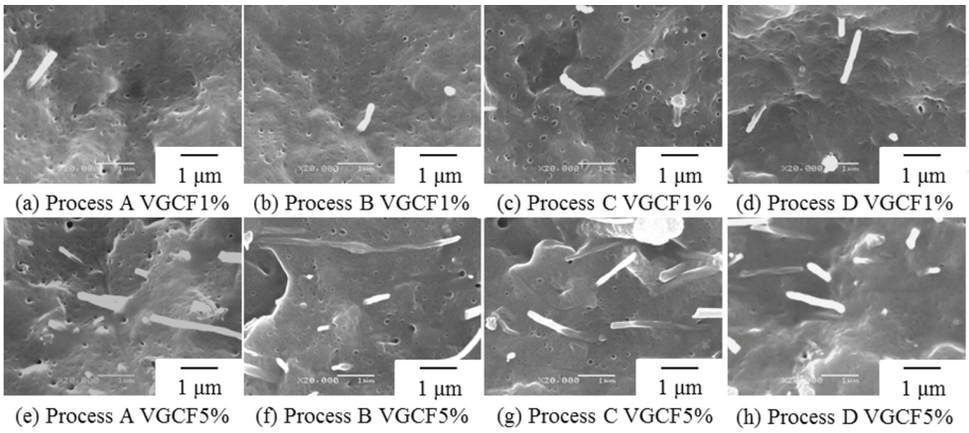

Figure 20. SEM micrographs of etched fracture surface for various processing sequence of the ternary composites (VGCF/PA6/SEBS-g-MA) (SEBS-g-MA content is 20 wt% and etched with toluene for 24 h to remove the dispersed phases): (a) Process A VGCF 1%, (b) Process B VGCF 1%, (c) Process C VGCF 1%, (d) Process D VGCF 1%, (e) Process A VGCF 5%, (f) Process B VGCF 5%, (g) Process C VGCF 5%, and (h) Process D VGCF 5%.

On the other hand, the dispersed SEBS-g-MA particles demonstrate good dispersion in the PA6 continuous matrix domains. **Table 7** summarizes the various data of the dispersed SEBS-g-MA particles in each ternary composites prepared by different processing sequences, which are calculated by image processing from SEM photographs such as number average diameter d_n, the weight average diameter d_w, the volume average diameter d_v, and polydispersibity d_w/d_n. The sizes of dispersed SEBS-g-MA particles change with the processing sequences and V_f, and these decrease fundamentally in the following orders: Process A > Process B > Process C > Process D. Thus, the size of dispersed SEBS particles values is closely related to the number of mixed SEBS-g-MA, and double mixing methods of SEBS-g-MA, which are the remixing of SEBS-g-MA such as processes C and D, are more effective than unimixing methods such as processes A and B. These behaviors may be attributed to the change in the mixing time, the physical interaction between PA6 and SEBS-g-MA, which is called as compatibilization effect, and also the dispersion and localization of VGCF; however, it is difficult to establish the exact reasons. Next, the number average fiber length l_n, weight average fiber length l_w, fiber distribution l_w/l_n, and number average aspect ratio $(a_r)_N$ are listed in **Table 8**. The number average aspect ratio $(a_r)_N$ is defined as l_n/d, where d is the average fiber diameter of VGCF ($d = \phi 150$ nm). The fiber length values of l_n, l_w, and $(a_r)_N$ generally decrease with increasing V_f except for process C, and the effect of processing sequences on the fiber length values decreases in the following orders: Process C > Process A > Process B > Process D. These behaviors may be attributed to the number of VGCFs mixed as mentioned earlier. In the case of process D, which is the first mixing step where VGCF was mixed with higher viscosity SEBS rather than PA6, enhances the damage of fiber in melt mixing.

Material		d_n (nm)	d_w (nm)	d_v (nm)	d_w/d_n
PA6/SEBS-g-MA (VGCF = 0%)		**88**	**97**	**121**	**1.11**
Process A	VGCF 1 vol%	81	88	104	1.08
	VGCF 5 vol%	51	59	95	1.17
Process B	VGCF 1 vol%	78	89	117	1.14
	VGCF 5 vol%	72	80	98	1.10
Process C	VGCF 1 vol%	68	77	102	1.12
	VGCF 5 vol%	52	55	66	1.07
Process D	VGCF 1 vol%	65	73	92	1.11
	VGCF 5 vol%	53	57	67	1.07

Table 7. Dispersed SEBS particle size of ternary composites (VGCF/PA6/SEBS-g-MA) prepared by different processing sequences.

Material		l_n (μm)	l_w (μm)	l_w/l_n	$(a_r)_N$
	VGCF 1 vol%	2.28	3.12	1.37	15.2
Process A					
	VGCF 5 vol%	2.22	2.96	1.33	14.8
	VGCF 1 vol%	1.78	2.54	1.43	11.9
Process B					
	VGCF 5 vol%	1.56	2.46	1.58	10.4
	VGCF 1 vol%	2.37	3.32	1.40	15.8
Process C					
	VGCF 5 vol%	2.39	3.32	1.39	15.9
	VGCF 1 vol%	1.63	2.08	1.28	10.9
Process D					
	VGCF 5 vol%	1.41	1.79	1.27	9.4

Table 8. Fiber length, its distribution, and aspect ratio of ternary composites (VGCF/PA6/SEBS-g-MA) prepared by different processing sequences.

To further clarify whether relationships between morphologies of ternary composites prepared by different processing sequences and dynamic viscoelastic properties of ones vary or not in this study, it is necessary to investigate the influences of the morphology of ternary composites on the dynamic viscoelastic properties in detail. G' is replotted as a function of average weight fiber length l_w in **Figure 21(a)** and the average weight diameter d_w in **Figure 21(b)**. In the figure, the number after each processing sequence code shows the volume fraction of VGCF in the composites. Generally, the fiber length dependence of G' slightly increases with l_w, and the influence of l_n on G' is smaller than that of V_f. These tendencies are related to the

processing sequence of remixing of VGCF (processes B and D). On the contrary, the diameter size dependence of G' increases with decreasing d_w. However, this relation is weaker than the processing sequence of remixing of SEBS-g-MA (processes C and D). It was found from these results that the dynamic viscoelastic properties of ternary composites prepared by different processes are closely related to their morphologies. In particular, processes B and D, which are the remixing methods of VGCF, have good dispersibility of VGCF which improves dynamic viscoelastic properties. However, the dynamic viscoelastic properties are not simply correlated with the fiber length of VGCF and diameter size of dispersed SEBS-g-MA particles. Therefore, further studies of how the relationships among dynamic viscoelastic properties, processing sequences, and morphologies of these ternary composites are determined should be conducted. The findings would not only contribute to the research of these ternary composites but also to other high performance polymer matrix composites.

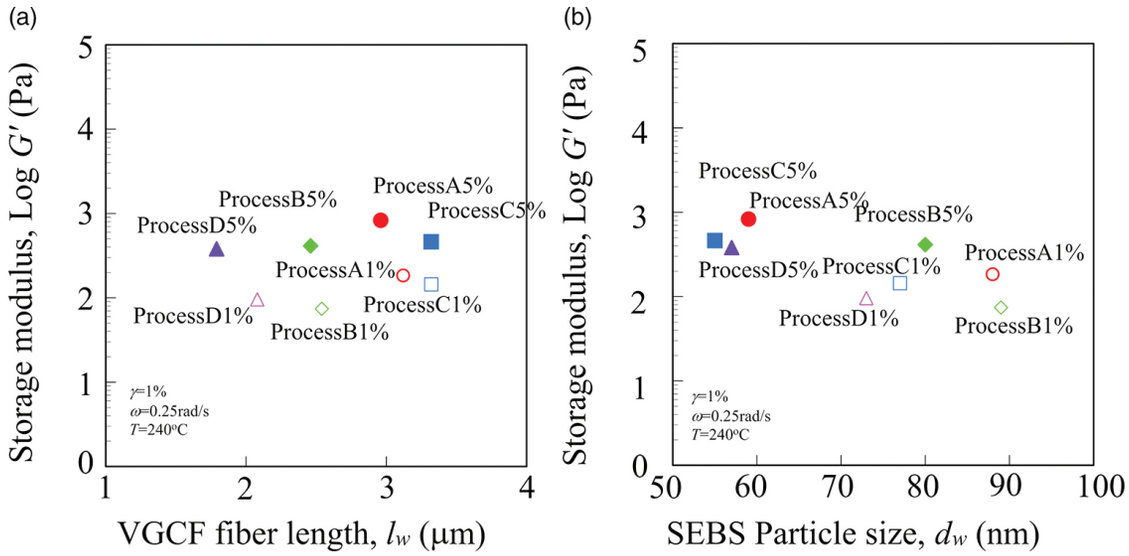

Figure 21. Influence of internal structure parameters such as SEBS particles size and fiber length on the storage modulus of various processing sequence of ternary composites (VGCF/PA6/SEBS-g-MA). (a) VGCF fiber length. (b) SEBS particle size.

5. Conclusion

We investigated the dynamic viscoelastic properties of carbon nanofiber (CNF)-filled polyamide composites and the blend of these composites and thermoplastic elastomer (TPE) in the molten state. In particular, this study discussed the effect of the addition of vapor grown carbon fiber (VGCF), which is a type of CNF, addition of TPE, and processing sequence on the dynamic viscoelastic properties in the molten state. It was found that VGCF has a stronger influence on the dynamic viscoelastic properties of the composites in the molten state. VGCF also has a high sensitive effect on the strain of transition from linear to nonlinear viscoelastic behavior, and the critical strain values at the transition decrease logarithmically with increasing VGCF

contents. Composites with lower VGCF content (1 vol%) showed lower dynamic viscoelastic properties (both storage and loss moduli) than those of pure PA66. However, the viscoelastic properties of composites with higher contents above 5 vol% increased rapidly with increasing VGCF content. From the results of various rheological behaviors, rheological percolation thresholds seem to exist between 1 and 5 vol% of VGCF contents. On the other hand, the effect of the addition of TPE on the dynamic viscoelastic properties of VGCF/PA6 composites in the molten state differed according to each viscoelastic value. It was clarified that the dynamic viscoelastic properties of VGCF/PA6/SEBS-g-MA ternary composites are higher than those of VGCF/PA6/SEBS ones. Furthermore, the influence of processing sequences on the dynamic viscoelastic properties of VGCF/PA6/SEBS-g-MA composites in the molten state differed according to mixing steps by materials. In particular, the viscoelastic properties of these ternary composites prepared by different processing sequences in the low angular frequency region changed with the processing sequences, which decrease in the following order: Process A > Process C > Process B > Process D. In particular, processes B and D are remixing methods of VGCF where VGCF is mixed twice, and are therefore more effective than unimixing methods such as processes A and C, and have good VGCF dispersibility which improves dynamic viscoelastic properties. These may be attributed to the change in the internal structure due to the addition of TPE, type of SEBS, and processing sequences.

Acknowledgements

We would like to thank the Functional Microstructured Surfaces Research Center (FMS, MEXT, Japan) of Kogakuin University, the Project Research of Research Institute for Science and Technology of Kogakuin University, and the Ogasawara Foundation for the Promotion of Science & Engineering for funding this study, and partial support by the national budget of Czech Republic within the framework of the Centre of Polymer Systems project (reg. number: CZ. 1.05/2.1.00/03.0111). The authors thank Mr. T. Natio, Mr. S. Togashi, Mr. Y. Takenaka, Mr. S. Sano, Mr. Y. Osada, and many master course and undergraduate course students at the Polymeric Materials Laboratory of Kogakuin University for their assistance with the experiments.

Author details

Yosuke Nishitani[1*] and Takeshi Kitano[2]

*Address all correspondence to: at13152@ns.kogakuin.ac.jp

1 Kogakuin University, Hachioji, Tokyo, Japan

2 Tomas Bata University in Zlin, Zlín, Czech Republic

References

[1] Paul D. R., Robeson L. M. Polymer nanotechnology: Nanocomposites. Polymer. 2008;49:3187–3204. DOI: 10.1016/j.polymer.2008.04.017

[2] Kim H., Abdala A. A., Macosko C. W. Graphene/polymer nanocomposite. Macromolecules. 2010;43:6515–6530. DOI: 10.1021/ma1005

[3] Spitalsky Z., Tasis D., Papagelis K., Galiotis C. Carbon nanotube–polymer composites: Chemistry, processing, mechanical and electrical properties. Prog. Polym. Sci. 2010;35:357–401. DOI: 10.1016/j.progpolymsci.2009.09.003

[4] Han Z., Fina A. Thermal conductivity of carbon nanotubes and their polymer nanocomposites: A review. Prog. Polym. Sci. 2011;35:914–944. DOI: 10.1016/j.progpolymsci.2010.11.004

[5] Gary G. T., Max L. L., Karla L. S., Brian P. R. A review of the fabrication and properties of vapor-grown carbon nanofiber/polymer composites: A review. Compos. Sci. Technol. 2007;67:1709–1718. DOI: 10.1016/j.compscitech.2006.06.015

[6] Iijima S. Helical microtubules of graphitic carbon. Nature. 1991;354:56–58. DOI: 10.1038/354056a0

[7] Endo M., Kim Y. A., Hayashi T., Nishimura K., Matusita T. Vapor-grown carbon fibers (VGCFs) basic properties and their battery applications. Carbon. 2001;39:1287–1297. DOI: 10.1016/S0008-6223(00)00295-5

[8] Caldeira G., Maia J. M., Carneiro O. S., Covas J. A., Bernardo C. A. Production and characterization of innovative carbon fiber–polycarbonate composites. Polym. Compos. 1998;19:147–151. DOI: 10.1002/pc.10085

[9] Hattum F. W. J. V., Bernardo C. A., Finegan J. C., Tibbetts G. G., Alig R. L., Lake M. L. A study of the thermomechanical properties of carbon fiber-polypropylene composites. Polym. Compos. 2000;21:970–977. Doi: 10.1002/pc.10391. 2000;21:970-977. DOI: 10.1002/pc.10391

[10] Carneiro O. S., Maia J. M. Rheological behavior of (short) carbon fiber/thermoplastic composites. Part I: The influence of fiber type, processing conditions and level of incorporation. Polym. Compos. 2000;21:960–969. DOI: 10.1002/pc.10249

[11] Carneiro O. S., Maia J. M. Rheological behavior of (short) carbon fiber/thermoplastic composites. Part II: The influence of matrix type. Polym. Compos. 2000;21:970–977. DOI: 10.1002/pc.10250

[12] Enomoto K., Yasuhara T., Ohtake N., Kato K. Injection molding of polystyrene matrix composites filled with vapor grown carbon fiber. JSME Intl. J. Series A. Solid Mech. Mater. Eng. 2003;46:353–358. DOI: 10.1299/jsmea.46.353

[13] Choi Y. K., Sugimoto K., Song S. M., Endo M. Mechanical and thermal properties of vapor-grown carbon nanofiber and polycarbonate composite sheets. Matter. Lett. 2005;59:3514–3520. DOI: 10.1016/j.matlet.2005.05.082

[14] Al-Saleh M. H., Sundararaj U. A review of vapor grown carbon nanofiber/polymer conductive composites. Carbon. 2009;47:2–22. DOI: 10.1016/j.carbon.2008.09.039

[15] Nishitani Y., Hirano Y., Ishii C., Kitano T., Sekiguchi I. Tribological properties of vapor grown carbon fiber filled polybutylene terephthalate composites. Mat. Technol. 2008;26:114–122.

[16] Nishitani Y., Ito J., Ishii C., Kitano T., Sekiguchi I. Tribological properties of vapor grown carbon fiber and carbon fiber reinforced polyimide composites. J. Mat. Testing Res. Assoc. Japan. 2009;54:12–23.

[17] Nishitani Y., Naito T., Kitano T., Sekiguchi I. Effects of addition of thermoplastic elastomers on tribological and mechanical properties of vapor grown carbon fiber filled polybutylene terephthalate composites. In: Proceedings of World Tribology Congress (WTC2009); 6–11 September; Kyoto 421. 2009.

[18] Naito T., Nishitani Y., Sekiguchi I., Ishii C., Kitano T., Sekiguchi I. Influence of addition of thermoplastic elastomers on mechanical and tribological properties of vapor grown carbon fiber filled polybutylene terephthalate composites. Seikei-Kakou (J. Japan Soc. Polymer Process.). 2010;22:35–47.

[19] Nishitani Y., Sekiguchi I., Kitano T. Rheological properties of various carbon fibers filled PBT composites. In: Proceedings of the Polymer Processing Society 26th Annual Meeting (PPS-26); 4–9 July, Banff, Canada. 2010. R01–134:1–9.

[20] Nishitani Y., Sekiguchi I., Ishii C., Kitano T. Dynamic viscoelastic properties of carbon nanofiber filled polyamide 66 composites in molten state. Mat. Technol. 2010;28:114–122.

[21] Nishitani Y., Togashi S., Sekiguchi I., Ishii C., Kitano T. Tribological properties of carbon nanofiber filled polyamide 66 composites. Mat. Technol. 2010;28:292–302.

[22] Nishitani Y., Sano S., Takenaka Y., Kitano T., Sekiguchi I. Effect of processing sequence on the mechanical and tribological properties of ternary composites (VGCF/PA6/SEBS-g-MA). J. Mat. Testing Res. Assoc. Japan. 2015;60:164–171.

[23] Hausnerova B., Honkova N., Lengalova A., Kitano T., Saha P. Rheology and fiber degradation during shear flow of carbon-fiber-reinforced polypropylenes. Polym. Sci. Series A. 2006;48:951–960. DOI: 10.1134/S0965545X06090100

[24] Hausnerova B., Honkova N., Lengalova A., Kitano T., Saha P. Rheological behavior of fiber-filled polymer melts at low shear rate Part. I. Modeling of rheological properties. Polimery/Polymers. 2008;53:507–512.

[25] Nishitani Y., Ishii C., Kitano T. Rheological properties of surface treated glass fiber reinforced polypropylenes in molten state, polypropylene. Dr. Fatih Dogan (Ed.); 2012.

Available from: http://www.intechopen.com/books/polypropylene/rheological-properties-of-surface-treated-glass-fiber-reinforced-polypropylenes-in-molten-state. DOI: 10.5772/35785

[26] Wu G., Asai S., Sumita M., Yui H. Entropy penalty-induced self-assembly in carbon black or carbon fiber filled polymer blends. Macromolecules. 2002;35:945–951. DOI: 10.1021/ma0104940

[27] Sumita M., Sakata K., Asai S., Miyasaka K., Nakagawa H. Dispersion of fillers and the electrical conductivity of polymer blends filled with carbon black. Polym. Bull. 1991;25:265–271. DOI: 10.1007/BF00310802

[28] Chow W.S., Ishak Z. A. M., Karger-Kocsis J., Apostolov A. A., Ishiaku U. S. Compatibilizing effect of maleated polypropylene on the mechanical properties and morphology of injection molded polyamide 6/polypropylene/organoclay nanocomposites. Polymer. 2003;44:7427–7440. DOI: 10.1016/j.polymer.2003.09.006

[29] Gonzalez I., Eguiazabal J. I., Nazabal J. Rubber-toughened polyamide 6/clay nanocomposites. Compos. Sci. Technol. 2006;66:1833–1843. DOI: 10.1016/j.compscitech. 2005.10.008

[30] Dasari A., Yu Z. Z., Yang M., Zhang Q. X., Xie X. L., Mai Y. W. Micro- and nano-scale deformation behavior of nylon 66-based binary and ternary nanocomposites. Compos. Sci. Technol. 2006;66:3097–3114. DOI: 10.1016/j.compscitech. 2005.10.008

[31] Nishitani Y., Ohashi K., Sekiguchi I., Ishi C., Kitano T. Influence of addition of styrene-ethylene/butylene-styrene copolymer on rheological, mechanical, and tribological properties of polyamide nanocomposites. Polym. Compos. 2010;31:68–76. DOI: 10.1002/pc.20767

[32] Nishitani Y., Yamada Y., Ishi C., Sekiguchi I., Kitano T. Effects of addition of functionalized SEBS on rheological, mechanical, and tribological properties of polyamide 6 nanocomposites. Polym. Eng. Sci. 2010;50:100–112. DOI: 10.1002/pen.21516

[33] Han C. D. Rheology and Processing of Polymeric Materials. In: Polymer Rheology, Oxford University Press. 2007; 1 Oxford, UK.

[34] Dasari A., Yu Z. Z., Mai Y. W. Effect of blending sequence on microstructure of ternary nanocomposites. Polymer. 2005;46:5986–5991. DOI: 10.1016/j.polymer.2005.05.145

[35] Gonzalez I., Eguiazabal J. I., Nazabal J. Effects of the processing sequence and critical interparticle distance in PA6-clay/mSEBS nanocomposites. Eur. Polym. J. 2008;44:287–299. DOI: 10.1016/j.eurpolymj.2007.11.027

[36] Tosaki M., Sakai H., Sasaki A., Takahashi Y., Matsubara M., Endo M. Rheological and mechanical properties of polypropylene filled with vapor-grown carbon fiber. Kobunsi Ronbunshu. 2005;62:585–590. DOI: 10.1295/koron.62.585

[37] Wang Y., Xu J., Bechtel S. E., Koelling K. W. Melt shear rheology of carbon nanofiber/polystyrene composites. Rheol. Acta. 2006;45:919–941. DOI: 10.1007/s00397-005-0077-8

[38] Durmus A., Kasgoz A., Macosko C. W. Linear low density polyethylene (LLDPE)/clay nanocomposites. Part I: Structural characterization and quantifying clay dispersion by melt rheology. Polymer. 2007;48:4492–4502. DOI: 10.1016/j.polymer.2007.05.074

[39] Wan T., Clifford M. J., Gao F., Bailey A. S., Gregory D. H., Somsunan R. Strain amplitude response and the microstructure of PA/clay nanocomposites. Polymer. 2005;46:6429–6436. DOI: 10.1016/j.polymer.2005.04.105

[40] Cassagnau P. Melt rheology of organoclay and fumed silica nanocomposites. Polymer. 2008;49:2183–2196. DOI: 10.1016/j.polymer.2007.12.035

[41] Ferry J. D. Viscoelastic Properties of Polymers. John Wiley & Sons, Incorporated; 1980 New York, USA.

[42] Nishitani Y., Sekiguchi I., Hausnerova B., Nagatsuka Y., Kitano T. Dynamic viscoelastic properties of long organic fibre reinforced polypropylene in molten state. Polym. Polym. Compos. 2001;9:199–211.

[43] Kitano T., Kataoka T. The effect of the mixing methods on viscous properties of polyethylene melts filled with fibers. Rheol. Acta. 1980;19:753–763. DOI: 10.1007/BF01521868

[44] Kitano T., Kataoka T., Nagatsuka Y. Shear flow rheological properties of vinylon- and glass-fiber reinforced polyethylene melts. Rheol. Acta. 1984;23:20–30. DOI: 10.1007/BF01333872

[45] Kitano T., Kataoka T., Nagatsuka Y. Dynamic flow properties of vinylon fibre and glass fiber reinforced polyethylene melts. Rheol. Acta. 1984;23:408–416. DOI: 10.1007/BF01329193

[46] Petra P., Fornes T. D., Paul D. R. Rheological behavior of multiwalled carbon nanotube/polycarbonate composites. Polymer. 2002;43:3247–3255. DOI: 10.1016/S0032-3861(02)00151-9

[47] Potschke P., Abdel-Goad M., Alig I., Dudkin S., Lellinger D. Rheological and dielectrical characterization of melt mixed polycarbonate-multiwalled carbon nanotube composites. Polymer. 2004;45:8863–8870. DOI: 10.1016/j.polymer.2004.10.040

[48] Kenneth S. C., Robert H. C. Dispersion and absorption in dielectrics I. alternating current characteristics. J. Chem. Phys. 1941;9:341. DOI: 10.1063/1.1750906

[49] Wu D., Wu L., Zhang M., Zhao Y. Viscoelasticity and thermal stability of polylactide composites with various functionalized carbon nanotubes. Polym. Degrad. Stab. 2008;93:1577–1584. DOI: 10.1016/j.polymdegradstab.2008.05.001

[50] Nishitani Y., Sekiguchi I., Hausnerova B., Zdrazilova N., Kitano T. Rheological properties of aminosilane surface treated short glass fibre reinforced polypropylenes.

Part 1: Steady shear and oscillatory flow properties in molten state. Polym. Compos. 2007;15:111–120.

[51] Kayatin M. J., Davis V. A. Viscoelasticity and shear stability of single-walled carbon nanotube/unsaturated polyester resin dispersions. macromolecules. 2009;42:6624–6632. DOI: 10.1021/ma901010d

[52] Van G. M., Palmen J. Time-temperature superposition for polymeric blends. Rheol. Bull. 1998;67:5–8.

[53] Meincke O., Kaempfer D., Weickmann H., Friedrich C., Vathauer M., Warth H. Mechanical properties and electrical conductivity of carbon-nanotube filled polyamide-6 and its blends with acrylonitrile/butadiene/styrene. Polymer. 2004;45:739–748. DOI: 10.1016/j.polymer.2003.12.013

[54] Trinkle S., Friedrich C. Van Gurp-Palmen-plot: A way to characterize polydispersity of linear polymers. Rheol. Acta. 2001;40:322–328. DOI: 10.1007/s003970000137

[55] Trinkle S., Walter P., Friedrich C. Van Gurp-Palmen Plot II? Classification of long chain branched polymers by their topology. Rheol. Acta. 2002;41:103–113. DOI: 10.1007/s003970200010

[56] Nishitani Y., Hasumi M., Kitano T. Influence of silane coupling agents on the rheological behavior of hemp fiber filled polyamide 1010 biomass composites in molten state [thesis]. In: AIP Conference Proceedings: 1664. Available from: http://dx.doi.org/10.1063/1.4918425

[57] Huang J. J., Keskkula H., Paul D. R. Rubber toughening of an amorphous polyamide by functionalized SEBS copolymers: Morphology and Izod impact behavior. Polymer. 2004;45:4203–4215. DOI: 10.1016/j.polymer.2004.04.002

[58] Balamurugan G. P., Maiti S. N. Influence of microstructure and deformation behavior on toughening of reactively compatibilized polyamide 6 and poly(ethylene-co-butyl acrylate) blends. Eur. Polym. J. 2007;43:1786–1805. DOI: 10.1016/j.eurpolymj.2007.02.035

[59] Nishitani Y., Kawahara T., Kitano T., Sekiguchi I. Effects of processing sequence on the physical properties of nanoomposites based on polyamide. In: Proceedings of Japan Society of Polymer Processing 2009 (Seikei-Kakou 09); 3–4 June 2009; Tokyo. 2009. pp. 181–182 (in Japanese).

[60] Tsurubuchi J., Naito T., Nishitani Y., Gotoh Y., Kitano T., Sekiguchi I. Effects of processing sequence on tribological properties of carbon nanofiber filled thermoplastic ternary composites. In: Proceedings of International Tribology Conference (ITC2011); 30 October–3 November 2011; Hiroshima. 2011. pp. P05–03:1.

[61] Fenouillot F., Cassagnau P., Majeste J.-C. Uneven distribution of nanoparticles in immiscible fluids: Morphology development in polymer blends. Polymer. 2009;50:1333–1350. DOI: 10.1016/j.polymer.2008.12.029

[62] Elias L., Fenouillot F., Majeste J.-C., Martin G., Cassagnau P. Migration of nanosilica particles in polymer blends. J. Polym. Sci. Part B: Polym. Phys. 2008;46:1976–1983. DOI: 10.1002/polb.21534

[63] Baudouin A.-C., Devaux J., Bailly C. Localization of carbon nanotubes at the interface in blends of polyamide and ethylene acrylate copolymer. Polymer. 2010;51:1341–1354. DOI: 10.1016/j.polymer.2010.01.050

IntechOpen